# UNIVERSITAT POLITÈCNICA DE VALÈNCIA

## Dept. of Communications

## Control of the electric response of dielectric nano-bars to create versatile reconfigurable metasurfaces.

Master's Thesis

Master of Science in Telecommunication Technologies, Systems and Networks

AUTHOR: Máñez Espina, Luis Manuel

Tutor: Sanchis Kilders, Pablo

Cotutor: Díaz Rubio, Ana

ACADEMIC YEAR: 2021/2022

**Objectives** – The objectives of this Master's Thesis can be condensed into three items:

- Concept demonstration of an all-dielectric full-transmission Huygens metasurface with reconfiguration capabilities consisting of infinite dielectric pillars with a slab of phase change material (PCM). Such a device should perform beam steering operations in the near-infrared (NIR) range with high energy efficiency.

- Study the electrical response obtained from the induced dipoles in the structure when modulating the PCMs refractive index.

- Develop a realistic design introducing the substrate that supports the dielectric metasurface and the losses the involved materials have approaching an achievable prototype.

**Methodology** – The methodology followed during this Master's Thesis consisted in:

1. Study and review of the related bibliography about metasurfaces.

2. Design of the chosen metasurface geometry following theoretical guidelines.

3. Development of COMSOL Multiphysics models to simulate the structure and study its scattering properties.

4. Optimization and parametrical study of the electromagnetic response using electromagnetic simulations.

**Results** – A full phase coverage was obtained using the PCM material as the active element of the metasurface. That led to the configuration of a high-efficiency reconfigurable metasurface capable of deflecting light to an anomalous angle. Several configurations were tested, and non-local behaviour was obtained. A realistic approach was developed by introducing the substrate and actual losses into the simulation. An almost complete phase range was obtained, indicating the possibility of creating an actual working prototype.

**Future lines** – This work serves as a demonstration of the working principle of a PCM-based reconfigurable metasurface. The last chapter of this thesis studies the possibility of using a GST material to build an actual experimental prototype. This last chapter is going to be used as a foundation to design a buildable device in the realm of the SURFING project(PID2021-128442NA-I00).

**Abstract** – For decades the manipulation of electromagnetic (EM) waves in the near-infrared has been a relevant topic in science and engineering. In recent years, the metasurface concept has emerged as a prominent, more compact and efficient solution to handling EM waves. Its applications in new technologies like LIDAR, FSO or highly sensitive sensors have led to an intense study of these devices. As a natural evolution of the technology, active reconfigurable metasurfaces were created. Using electromagnetic simulation software, this work shows the implementation of a phase change material (PCM), a material that can modulate its refractive index, as the active component of the metasurface. The studied metasurface geometry consists of an array of infinite dielectric bars with a slab of PCM inside. Its scattering response relies only on the induced electric dipole resonances. A full phase coverage in transmission is proven possible leading to the development of different reconfigurable settings with high energy efficiency. Furthermore, a buildable prototype is simulated, taking into account the constraints imposed by real materials. The chosen PCM material is part of the GST family, the substrate is made of calcium fluoride, and the main structure uses germanium.

Autor: Luis Manuel Máñez Espina, email: lmmaeesp@teleco.upv.es
Director 1: Pablo Sanchis Kilders, email: pabsanki@ntc.upv.es
Director 2: Ana Díaz Rubio, email: andiaru@upv.es
Fecha de entrega: 04-09-2022

# Contents

# 1    Introduction

Throughout history, the manipulation and control of electromagnetic (EM) waves have been active and relevant topics for scientists and engineers. The creation of devices capable of that comprehensive task is crucial in the development of communication systems. In recent years, the general interest in communications has shifted towards higher frequencies, allowing broader bands and more data capacity. Specifically, exploiting the Near-infrared (NIR) spectrum (ranging from 0.8-2.5 $\mu$m wavelength) has been a hot topic in science in the last decades due to its applications in LIDAR, free space communications, fiber optics and photonics, among other fields. In this sense, significant progress has been made in developing NIR sources and detectors. However, controlling the amplitude and phase of the scattered light at these frequencies is still an open subject. Another well-known issue is the difficulty in the miniaturization of devices working at such frequency bands and, in general, at optical frequencies. In order to overcome these limitations, the development of metasurfaces arose as a solution.

Nature provides materials with a wide range of electric and magnetic responses. Although this diversity exists, not all possible electromagnetic behaviours are found. This limitation complicates the manipulation of EM waves, especially at high frequencies. At the beginning of the 2000s, scientists started to develop new materials that macroscopically had EM responses that were not found in nature. These new materials were formed by subwavelength size periodically spaced structures made of classical materials. Each structure component receives the name of meta-atom, as it acts as an atom in conventional matter structures. Following the analogy, the word metamaterial was created to designate all the artificially made three-dimensional structures formed by meta-atoms that controlled light as desired. The research field of metamaterials was intensively active in its early stage, but the intrinsic complications of engineering these materials and their bulkiness led to the exploration of a two-dimensional version of the same idea. Moreover, these new surfaces were intended to have complete control over EM waves with almost negligible thickness. They were attributed with the name metasurfaces.

Initially, the idea of a metasurface was realised using plasmonic structures made by metal-made meta-atoms. Such systems turned inefficient and did not provide full phase coverage by themselves [1]. Researchers tried to solve these problems by using dielectric subwavelength meta-atoms. A near-unity transmittance and full $2\pi$ phase coverage were achieved with a dielectric meta-atoms structure [2]. Nowadays, one of the main goals in the field is the creation of reconfigurable metasurfaces [3], devices that can change their response via an external signal. There are many paths to achieve that goal: mechanical actuation [4], electrical gating [5], photocarrier excitation, phase-change materials [6] and any other way to change the EM characteristics or geometry of the metasurface or its surroundings. Current interest in this research field is the creation of reconfigurable metasurfaces using Phase Change Materials (PCM) as the dynamical element. Especially non-volatile PCMs, which after being excited, stay in a specific state, holding their electromagnetic properties without the need for continuous excitation [7].

This master thesis will cover the theoretical study of a reconfigurable metasurface that uses a PCM as its active element. At first, It will be shown how by changing the refractive

index of the PCM in the metasurface, full phase coverage can be achieved by the device. This will lead to the opportunity of steering light beams with different configurations of meta-atoms. The properties and phenomena that govern these interactions will be studied.

# 2    Objectives

The main objective of this work is the theoretical development of a reconfigurable metasurface, designed to perform in the near-infrared (NIR) range with high energy efficiency, using electromagnetic simulation software and the study of the theoretical physical phenomena involved. This task is going to be divided into several steps:

- Design of a one element periodical array of infinite dielectric bars. Identification of the different resonances and their behavior when an active element, a phase change material, is introduced.

- Achieve full-phase coverage with almost full transmission by modulating the refractive index of the active material in the metasurface.

- Use the known theoretical results to developt a reconfigurable metasurface with simple beam steering capabilities.

- Approach to a buildable device. Realistic simulations for a near buildable prototype configuration.

# 3    Theoretical background

In general, Maxwell equations and boundary conditions are sufficient to calculate the fields for any given electromagnetic problem. If we could solve every partial differential equation (PDE) analytically, electromagnetism would be an overcame field of physics. However, the reality is far from that. The set of analytically solvable PDEs is infinitely smaller than the set of existing PDEs, and for this reason scientists and engineers are actively working to provide new methods to solve electromagnetic problems. Although nature is intrinsically complex, it becomes simple and arguably beautiful in some scenarios. These cases are studied because they are the most apprehensive situations that can aid in understanding non-analytically solvable problems. Most of these problems have something in common, symmetries. This is the case of metasurfaces, where the periodic distribution of the inclusions in space allows to use of some theoretical assumptions to simplify the problem, revealing the physical phenomena hidden in this type of structure. In this section, with the purpose of providing to the reader the necessary theoretical aspects to understand this work, a brief discussion of the ground concepts that are going to be used in future chapters is presented.

## 3.1 Floquet Theorem

As mentioned before, metasurfaces, by definition, have at least translational symmetry. That is a direct consequence of the periodicity of the structure. Mathematically one could describe this property as:

$$u(\vec{r} + \vec{D}) = u(\vec{r}), \tag{1}$$

with $\vec{D}$ being the vector that defines the periodicity in a given direction and $u$, any physical quantity. This geometrical constraint carries out several consequences. The most important one is in the solution's form of the electromagnetic fields.

Gaston Floquet, in the 19th century, studied differential equations and discovered that the solutions of equations fulfilling this boundary condition (i.e. periodicity) could not be arbitrary and that they had certain properties. For the sake of clarity, the consequences of this mathematical discovery will be tackled in the mathematical form that is useful for electromagnetism and not in its original state, that treats general differential equation systems [8].

Assume that a flat structure with a fixed periodicity $D$ is illuminated with a plane wave with an incident angle $\theta_i$. The size of the period is that of the unit cell of the structure. The periodicity of the structure ensures that the fields at an arbitrary point $x$ are the same as those found at $x + D$, except for the phase difference of the incident wave given by $\Delta\phi = -k_0 \sin(\theta_i)D$, where $k_0$ is the wavevector in free space. The following mathematical equality holds in the tangent direction of the periodic structure, assuming a one-dimensional periodicity, $u(x) = e^{jk_o \sin\theta_i D}u(x + D)$, where $u$ represents the spatial distribution of the electric or magnetic field components. Using the auxiliary equation $Q(x) = e^{jk_o \sin\theta_i x}u(x)$ that inherits the periodicity of the structure, a Fourier series expansion is possible and reads

$$Q(x) = \sum_{n=-\infty}^{+\infty} p_n e^{-j\frac{2\pi n}{D}x}, \tag{2}$$

where $p_n$ represents the complex amplitudes of the Fourier harmonics and $n$ the order of the harmonic. Using this expression, the spatial distribution $u(x)$ can be written as

$$u(x) = \sum_{n=-\infty}^{+\infty} p_n e^{-j(k_o \sin\theta_i + \frac{2\pi n}{D})x}. \tag{3}$$

From Eq.3, it is visible that $u(x)$ is formed of an infinite number of modes, which are called Floquet modes. The $n$-th mode propagates with a transverse wavevector $k_{xn} = k_o \sin\theta_i + \frac{2\pi n}{D}$ and complex amplitude $p_n$. In free space, the dispersion relation is $k_0^2 = k_{nx}^2 + k_{zn}^2$. The normal component $k_{zn}$ is uniquely determined by the incident wavevector and the possible values of the transversal component. A concrete Floquet mode will propagate if both components of the $k_n$ vector are real. Analyzing the expression for $k_{xn}$, it is visible that this component is always real. However, when $|k_{xn}| > k_0$, the $k_{zn}$ component will be imaginary, and the mode will be evanescent.

From this result, it can be stated that for structures with an under-subwavelength period, only the first Floquet mode will propagate. Then these structures can be modelled by the surface-averaged and uniformly distributed surface currents if what we search is for the far field distributions. This case of arrangement is called homogenizable [9]. Assuming the extreme case of $k_{x1} = k_0$, the condition for no higher order propagation is not satisfied. As a result, the condition for having only one propagating mode, known as the *diffraction limit*, reads: $D < \lambda/(1 + \sin\theta_{\mathrm{i}})$.

## 3.2 Diffraction Orders and the generalized law of reflection and refraction

A valid way of explaining the interaction between a thin layer of material that holds a periodic structure and light, is using the concept of diffraction modes. When light is diffracted by a structure that is periodically repeated, called diffraction grating, the different paths taken can conclude in destructive or constructive interactions. As the Huygens-Fresnel Principle states, each point on a wavefront can be considered a new wave source point, and a wavefront in any subsequent point can be found adding all the contributions made by the point wave sources of the previous wavefronts. Using the Huygens principle, we can trace the paths that light can take and calculate the phase differences. For a diffraction grating with period $D$, the angles with maximum constructive interference will be those that satisfy

$$D(\sin\theta_{\mathrm{i}} - \sin\theta_m) = m\lambda, \tag{4}$$

where $\lambda$ is the wavelength in the propagation media, $\theta_m$ is the exit angle, and $\theta_{\mathrm{i}}$ is the angle of incidence. The parameter $m$ is an integer that is called the diffraction order and it coincides with the Floquet mode order. The zero diffraction order is an interesting case because it represents the usual diffraction and reflection behaviours. From Eq.4 it can be seen how with a fixed wavelength, a greater period makes higher diffraction orders possible. When multiple modes can propagate, the properties of the grating will determine how the energy is coupled to each mode.

Recently, the development of metasurfaces has led to a different approach to explaining the same phenomena. Metasurfaces are thin compared to the wavelengths that they are created to work. Most of them could be modelled as an infinitely thin sheet. Taking the Fermat principle, that states that from all the possible paths, light travels the fastest possible one. And modelling the metasurface as a device that is between two mediums and that only contributes to the light path as a phase change, the next equation is achieved [10]

$$n_t \sin\theta_t - n_i \sin\theta_i = \frac{\lambda_0}{2\pi}\frac{d\Phi(x)}{dx}, \tag{5}$$

where $n_t$ and $\theta_t$ are the refractive index of the second medium and the angle between the normal and the transmitted ray, respectively. Whereas $n_{\mathrm{i}}$ and $\theta_i$ are the refractive index of the first medium and the angle of the incident ray.

This result is usually called the "Generalized Law of Refraction" [1]. For Eq. 5 to be true, the function has to be linear, then the derivative is a constant magnitude. The first conclusion that one can extract from the equation is the possibility of achieving an extraordinary, different from the usual diffraction, exit angle by changing the phase gradient of the metasurface. In reality, the only way of achieving an infinite phase gradient is that of a periodic structure. Exploiting that $\Phi = \Phi + 2\pi k$ with $k$ an integer, a triangular shape phase profile is necessary to fulfil the constant phase gradient condition. The expression of the gradient is reduced to $d\Phi/dx = \pm 2\pi/D$.

Devices with such profiles already exist and are usually called blazed gratings. Blazed gratings are a special case of diffraction gratings, they are optimized to couple light to one particular diffraction order by using a slope-looking profile. Although the approach is different from what was shown with Floquet's theorem, the result is that the generalized law of diffraction is only a way of coupling the energy to the first diffraction order using the same strategy as blazed gratings do [11]. The biggest advantage of Eq.5 is that it elegantly displays a way of beam steering. A change in the phase gradient of the structures leads to a change in the exit angle.

In the design that we are going to study, the generalized law of diffraction is used to explain how changing the refractive index of the structure elements, a beam steering effect can be achieved. Another way of explaining this effect is by an analogue to what an array of antennas can achieve if their relative phase is modulated. A shift in the relative phase of the antennas that form the array leads to a change in the beam pointing direction. Eq.5 is a continuous and periodic expression of that same effect for subwavelength "antennas". In the metasurfaces case these are scatterers.

## 3.3 Homogenization models for metasurfaces

In general, and thanks to the subwavelength dimensions of the meta-atoms, homogenization models can be used to describe the properties of metasurfaces by general macroscopic quantities. In addition, a metasurface is homogenizable only if one Floquet mode propagates in the far field and the period is deeply subwavelength. There are various popular homogenization schemes. In this section, a brief introduction to the polarizability model will be explained. This model relates incident fields with electric and magnetic polarizations in the metasurface, which lead to effective magnetic and electric currents that serve as the sources of the scattered fields. The polarization of the structure is equivalent to thinking in terms of induced magnetic and electric dipoles being excited by the incident fields. This way of visualizing the effect will be used during this master's thesis due to its convenience when qualitatively trying to understand the physical problem.

In terms of the incident magnetic field $\mathbf{H}_i$ and electric field $\mathbf{E}_i$, a first order approximation to the expression for the polarizability is

$$\mathbf{p} = \bar{\bar{\alpha}}_{ee}\mathbf{E}_i + \bar{\bar{\alpha}}_{em}\mathbf{H}_i, \qquad \mathbf{m} = \bar{\bar{\alpha}}_{me}\mathbf{E}_i + \bar{\bar{\alpha}}_{mm}\mathbf{H}_i. \tag{6}$$

where the $\bar{\bar{\alpha}}$ are tensors called collective polarizabilities because they depend on the geometry and material of each meta-atom, and in the periodical array. The subscripts

make reference to the electric and magnetic components of each contribution. The cross terms of the collective polarizability measure the coupling between the incident electric and magnetic field and the cross fields in the scattering response. A $\bar{\bar{\alpha}}_{em} \neq 0$ and/or $\bar{\bar{\alpha}}_{me} \neq 0$ shows a coupling between the magnetic and electric fields from the incident wave and the scattered by the structure. That effect is known as bianisotropy and makes possible, for example, the rotation of the polarization by isotropic materials.

From the above expression for the induced electric and magnetic moments, one could easily calculate the equivalent currents caused by the incident field. The obtained currents will determine the forward and the backward scattered field. A schematic of this scenario will be considered Fig.1. The incident field with wavevector $\mathbf{k}_i$ is a planewave that fills all the space. The two-dimensional sheet, modelled by its induced currents, produces the scatter fields labelled as $\mathbf{E}_b$ for backward scattering and $\mathbf{E}_f$ for forward scattering. Using the homogenization model presented in Eq. 3.3, the induced currents in the metasurface are directly calculated by

$$\mathbf{J}_e = \frac{jw\mathbf{p}}{S}, \qquad \mathbf{J}_m = \frac{jw\mathbf{m}}{S}, \tag{7}$$

where $S$ is the unit cell area. The calculated electric fields would follow the next expressions

$$\mathbf{E}_f = -\frac{\eta}{2}\mathbf{J}_e \mp \frac{1}{2}\mathbf{n} \times \mathbf{J}_m, \qquad \mathbf{E}_b = -\frac{\eta}{2}\mathbf{J}_e \mp \frac{1}{2}\mathbf{n} \times \mathbf{J}_m. \tag{8}$$

Combining these two, the fields that are reflected and transmitted can be expressed as:

$$\mathbf{E}_r = -\frac{jw}{2S}(\eta\mathbf{p} \mp \mathbf{n} \times \mathbf{m}), \qquad \mathbf{E}_t = \mathbf{E}_i - \frac{jw}{2S}(\eta\mathbf{p} \pm \mathbf{n} \times \mathbf{m}). \tag{9}$$

The top case for the sign in the previous equations denotes an election of normal vector in the opposite direction that the incident wavevector $\mathbf{k}_i$. The bottom case is for a situation where both vectors are pointing at the same direction.
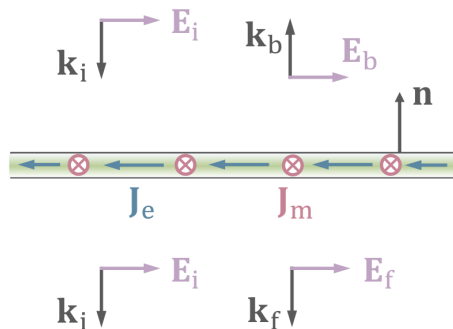


**Figure 1:** Field configuration for a metasurface scattering problem. Extracted from [8]

## 3.4  Full-transmission conditions and Huygen's metasurfaces

For some applications, a full-transmission response with phase control could be desired. The first requirement that has to be fulfilled is that the materials used in the configuration

have to be lossless at the working frequency. In that sense, the natural selection for this type of metasurfaces, at the NIR range, are high refractive index near lossless materials, like Germanium or Silicon.

When a dielectric structure is illuminated by a plane wave, three principal types of scattering can occur depending on its size and the wavelength used. In the case of subwavelength dielectric particles, the predominant effect is the Mie scattering. These particles are said to have Mie resonances. Although Mie scattering makes reference to the solutions of the fields of spherical particles being radiated by plane waves, the term is also used for the kind of EM fields that are produced by other dielectric subwavelength structures excited by plane wave radiation. The most interesting result that can be extracted from the Mie Theory is that the scattering cross section can be expressed by closed terms that depend on the Mie coefficients. These coefficients depend on the geometry and composition of the scatterers. The expression for the back and forward scattering cross section for a spherical dielectric particle is as follows

$$C_s^f = \frac{1}{a^2 k^2}\left|\sum_{n=1}^{\infty}(1+2n)(-1)^n(a_n - b_n)\right|^2, \qquad C_s^b = \frac{1}{a^2 k^2}\left|\sum_{n=1}^{\infty}(1+2n)(a_n + b_n)\right|^2, \quad (10)$$

where $a_n$ and $b_n$ are the Mie coefficients of $n$-th order and $a$ is the radius of the sphere. Similar mathematical expressions can be extended to other geometries [12].

Taking into account only the first order, doing what is called the dipole approximation (i.e. neglecting higher order contributions), it can be worked out the condition for minimum backscattering. Mathematically, this condition is only that $a_1 - b_1 = 0$. Physically, this is translated as the structure behaving as a pair of magnetic and electric dipoles that oscillate in phase and with the same magnitude in normal directions. The stated condition is usually referred to as the first Kerker condition. The sum of both dipoles is called a Huygens source because it works like a perfect source in the wavefront just like a new point in the path of a plane wave. Metasurfaces whose meta-atoms behave as induced pairs of normal dipoles are usually called Huygens metasurfaces [13].

The combination of the periodical boundary condition, which makes only possible Floquet modes to propagate, and the addition of the resonance requirements for full transmission explains the results that are going to be covered in the next sections. Following the idea of achieving full transmission by creating Huygens metasurfaces, it can be worked out that to achieve zero backscattering it is a necessary condition to excite scattering modes with opposite symmetries. From Eq.(10) we know that a superposition of a magnetic dipole and a normal electric dipole is sufficient to have zero backscattering. But that is not the only way of achieving it. Another example of a full transmission device is that of the superposition of two electric dipoles normal to each other [14]. In general, the superposition of symmetric and antisymmetric scattering sources in phase and with the same magnitude is sufficient for zero backscattering, if they are properly oriented.

# 4    Analysis of one element metasurface

The presented metasurface consists of rectangular section bars of dielectric material. The bars are considered to be infinite in the $y$-direction and are placed in parallel with a period $D$, see Fig.2. The infinite assumption is valid for this case due to the NIR wavelengths in use and the usual size of construction of photonic devices in comparison. The bars are conformed of high refractive index dielectric material with low losses in the NIR. A slab of phase change material (PCM) will be used to achieve reconfigurability. In this section, the dielectric materials are considered to be lossless therefore modelled by a real refraction index. The topology used in this analysis is known to hold electric and magnetic resonant modes [14]. As discussed in the previous section, these modes are generated via the electric and magnetic field induced inside the high-refractive index structure. They are also known as Mie-type resonances which are strongly dependent on the size structure and geometry.

The structure will be considered to be made of germanium. The experimentally calculated refractive index in the used NIR band for germanium is approximately 4. Using such a refractive index raises some problems. It is not sufficiently large to confine the electromagnetic waves efficiently. Moreover, phenomena like non-local effects are more prominent to arise. The slab of PCM will be modelled as a perfect behaving piece of material that can achieve any refractive index in a given range without losses. In the last sections, the material will be modelled more realistically. The design parameters are defined as: $w$ for the x-dimension of the dielectric bars, $h$ for the z-dimension of the dielectric bar and for $D$ for the period of the array, see Fig.2.

The resonant modes that appear in the dielectric bars can be modelled using induced dipole moments. It is conceptually easy to visualize that in a rectangular section of dielectric material excited by a plane-wave with an in-plane electric field and with $\mu = 1$, the only possible first order induced dipoles are the $x$ and $z$ electric dipoles and a $y$-oriented magnetic dipole. The explanation for the three resonant modes is as follows: the induced electric dipoles are directly caused by the electric field inside the structure pointing in the same direction; the induced magnetic dipole is caused by the circulation of the electric field, as Lenz's law states. The structure will also hold superpositions of the mentioned modes. The restriction to dipole moments instead of higher order moments will be confirmed by analyzing the far fields obtained.
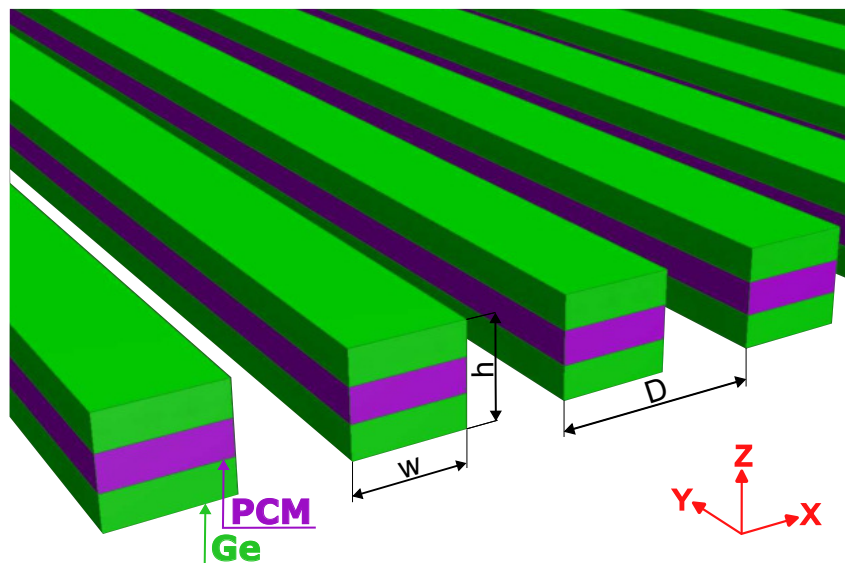
**Figure 2:** 3D representation of the all-dielectric infinite bars metasurface. The design parameters are depicted in the figure: $D$ for the periodicity of the structure, $w$ for the width, and $h$ for the height of each dielectric pillar. The green colour material is Germanium, with refractive index $n_d$, and the purple colour material is the PCM, that will make possible the reconfiguration of the metasurface, with refractive index $n_{PCM}$. The height of the PCM slab is 1/3 of the height of the structure, $h_{PCM} = 1/3h$. This feature will be carried along all this masters thesis unless is explicitly redefined.

Full control of the response can only be achieved with a one element unit cell metasurface that can be tuned and covers the entire $2\pi$ phase range. This section will cover the identification of the different resonant modes and the configuration of full transmission, and total phase coverage, on a one-element meta-atom metasurface.

## 4.1    Resonant Modes and Response Reconfigurability

When the structure is illuminated obliquely, the electric field excites the structure in $x$ and $z$ directions. Thus with the given incidence, up to first order, three main resonant modes are excited in the rectangular cavity. Fig.3a represents the reflectance, $|S_{1,1}|^2$, of the structure. The three resonances are shown when the incident angle is $\theta_i = 45°$, each of them reaching perfect reflection. The first resonance Fig.3b, centred at 115 THz is a y-directed magnetic dipole. The circulation of the electric field can be observed in the figure. The second resonance Fig.3c, which is centred at approximately 150 THz is an electric dipole in the x-coordinate. The last resonance is placed at 175 THz and depicts a z-oriented electric dipole.

Introducing the phase change material (PCM) slab allows the structure to change its refractive index and thus alter the way in which the metasurface interacts with light. The structure will have a layer of PCM centred in the dielectric bar, with a height of 1/3 of the total, as it is shown in Fig.2. Variations of the refraction index of the PCM

layer significantly affect both electric dipole resonances. A higher/lower diffraction index means higher/lower confinement creating a shift in the frequencies in which the resonances occur. The change of the refractive index implies a change in the electric dimensions of the structure: for higher/lower indexes, bigger/smaller electric dimensions that interact with longer/shorter wavelength (higher/lower frequencies).

Although full transmission and phase control can be achieved using a magnetic and electric dipole [6], in this case, using two orthogonal electric dipoles will be sufficient due to their symmetric and antisymmetric electric field distributions in the z-direction [14].
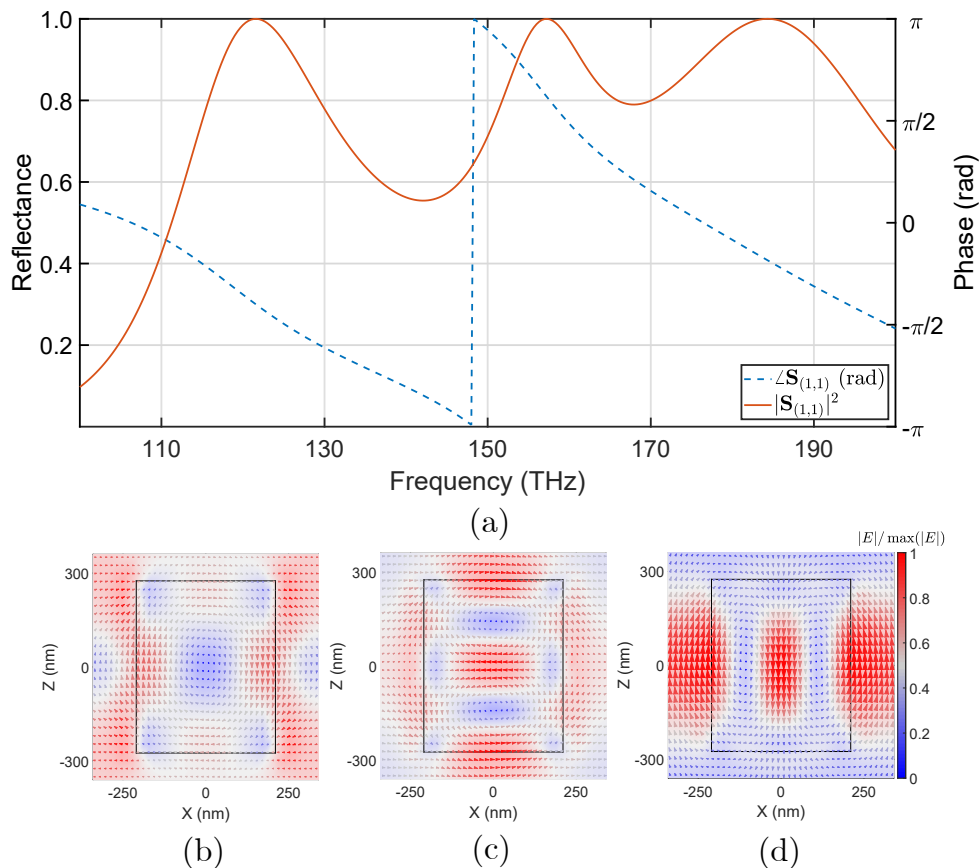


(a)



(b)              (c)              (d)

**Figure 3:** One element metasurface. (a) Reflectance of the dielectric structure with $D = 800$nm, $w = 420$nm, and $h = 550$nm when $\theta_i = 45°$. The refractive index are $n_d = n_{PCM} = 4$. The three electric field distributions for the resonant modes are: (b) at 115 THz for the magnetic dipole in the z-direction, (c) at 150 THz for the electric tangential dipole and (d) at 175 THz for the vertical electric dipole.

The resonances must shift at different rates when the PCM index is modulated to change the relative phase of the meta-atoms. Fig.4 shows the shift in the resonance frequencies when the refraction index of the PMC changes. As mentioned earlier, Fig.4a shows how a greater refractive index of the PCM shifts resonances to lower frequencies. In the same fashion, Fig.4b shows that smaller values of $n_d$ shift resonances towards higher frequencies.
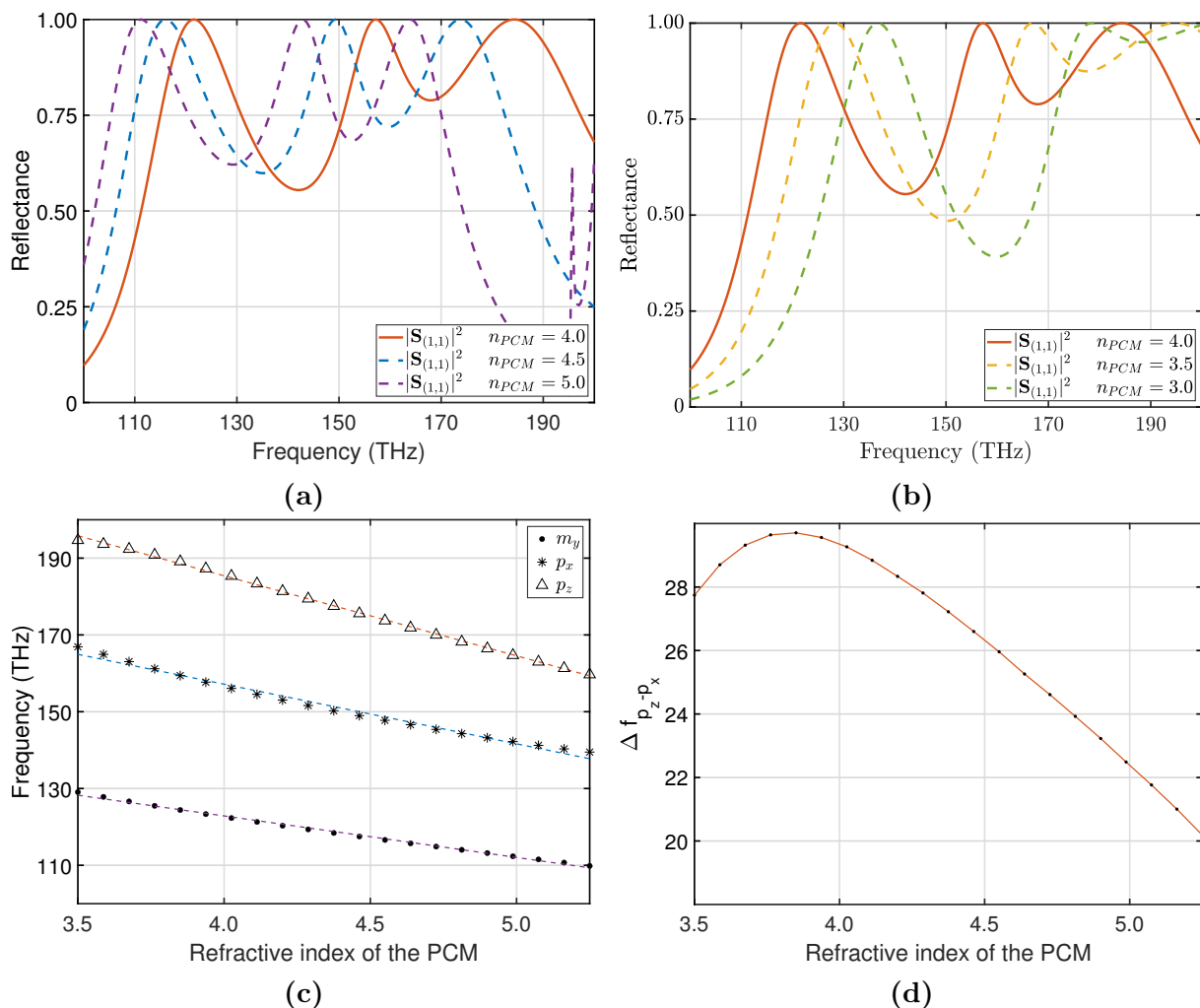
**Figure 4:** The reflectance of the structure as a function of the frequency for multiple values of $n_{PCM}$ is depicted in (a) and (b), the orange line represents the homogeneous case where $n_d = n_{PCM} = 4$. (c) Shows the evolution of each resonance central frequency when $n_{PCM}$ is modulated. It has been assumed that the resonances are Lorentz functions. (d) The representation of the relative distance between the electric dipole modes as a function of the PCMs refractive index, $n_{PCM}$. All the results where obtained for a fixed $n_d = 4$ and $\theta_i = 45$ and with geometrical parameters $D = 800$nm, $w = 420$nm and $h = 550$nm

In Fig.4c The evolution of the centre of each resonance is shown. All three resonances have linear behaviour to the refractive index. The dashed lines show the values of the linear fit, the three of them with $R^2$ values higher than 0.999. Fig.4d shows the relation between the refractive index of the PCM and the relative position of the electric resonances. It is not constant. Thus a relative shift that would carry a phase range coverage is possible. The phase is also affected by the change in the PCM. At a fixed frequency, the functional relation between the refractive index and the phase is inverse, Fig.5, as in the frequency shift case for the resonance reflection.
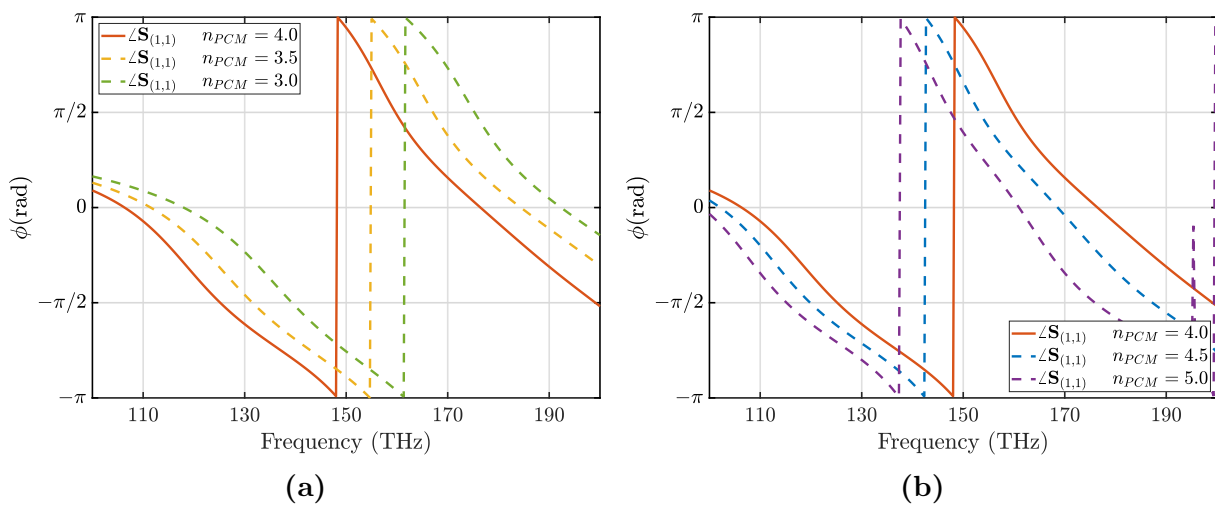
**Figure 5:** Phase of the scattering parameter $\mathbf{S}_{1,1} = r$, being $\mathbf{r}$ the reflection coefficient, as a function of the frequency for multiple values of $n_{\mathrm{PCM}}$. All the results where obtained for a fixed $n_{\mathrm{d}} = 4$ and $\theta_{\mathrm{i}} = 45$ and with geometrical parameters $D = 800\mathrm{nm}$, $w = 420\mathrm{nm}$ and $h = 550\mathrm{nm}$

## 4.2    Full Transmission and Phase Modulation

The constitution of a full transmission metasurface is only possible if the scattered fields in the backward direction interfere in a destructive manner. This can be achieved by superposing a symmetrical and antisymmetrical response in the device scattering fields [14]. The destructive interaction is achieved in the present case by superposing the two orthogonal electric dipole resonances and creating an electric dipole oriented at $45^{\mathrm{o}}$. To achieve the perfect coupling of both resonances, the dimensions in height and width have to be similar.

Fig.6 shows how the change in the geometrical parameter $h$ brings closer the electric dipole resonances ending up with a full transmission Huygens metasurface. The blue line is the same case as in Fig.3, while the last green dashed line is the same case as in Fig.7. Only the reflectance is shown in the graph to maintain clarity.
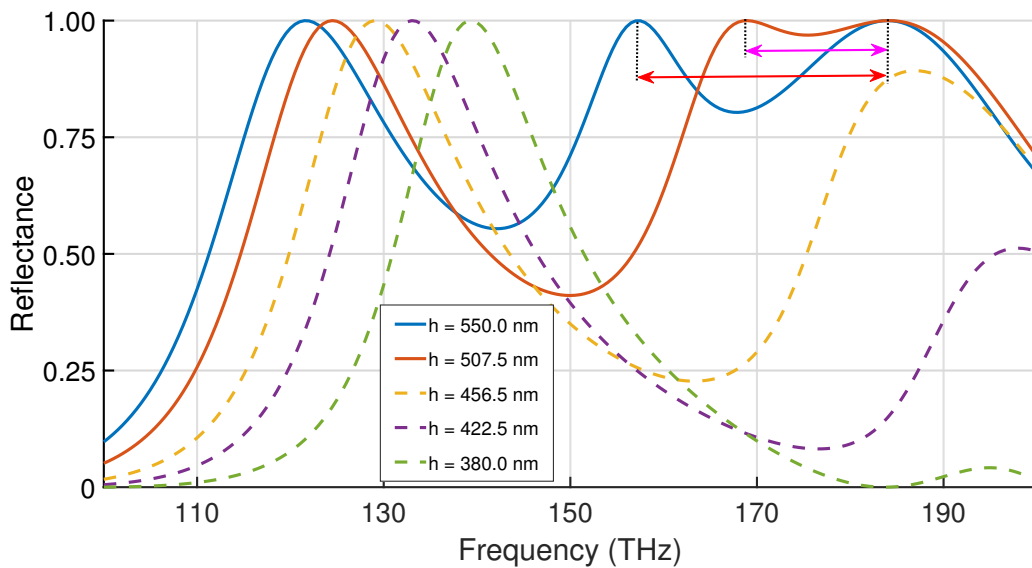
**Figure 6:** At a fixed $w = 420$nm and $D = 800$ nm, with an homogenous dielectric bar with $n_d = n_{\text{PCM}} = 4$ as in Fig.3, the $h$ parameter is changed between 550 nm and 380 nm. The reflectance values of the structure are depicted as a function of the frequency. The angle of incidence is $\theta_i = 45$.

When $\theta_i = 45°$, the angle of incidence of the plane wave provides the same amount of polarization excitation to the dielectric structure in the $z$ and $x$ directions. However, due to the effects of interaction between the periodically disposed bars, the optimal height and width are not the same as it would be what intuitively one could think. Fig 7a shows the reflectance, transmittance and phase of the metasurface when the electric dipoles have the same amplitude and are centred around the same frequency. The metasurface behaves as a Huygens metasurface around 190 THz, achieving full transmission. Interesting to point out that the magnetic resonance is still happening at 135 THz. The tune is made for $n_{\text{PCM}} = 4$ (i.e. an homogeneous dielectric bar). Fig.7b shows the electric field distribution at 200 THz where it can be seen how the combination of both resonances induces a $45^{\text{o}}$ oriented electric dipole that enables full transmission. This Huygens metasurface has been achieved using the superposition of a symmetric and antisymmetric dipole resonance, following the idea shown in [14].
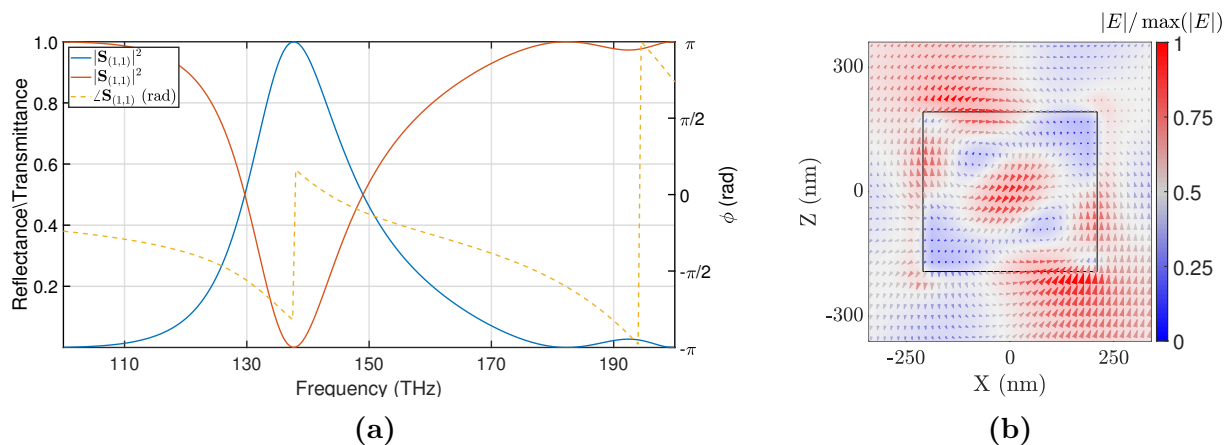
**Figure 7:** (a) Transmittance and reflectance of a syntonized full-transmission high dielectric index metasurface. The dimensions of the rectangular section bars are $w = 420$nm and $h = 385$nm, with a periodicity of $D = 800$nm and $n_\mathrm{PCM} = n_\mathrm{d} = 4$. (b) Electric field distribution at 200THz, showing the electric dipole oriented at $45^\mathrm{o}$ with respect of the x-axis achieving full transmission as in [14]. The planewave angle of incidence is $\theta_\mathrm{i} = 45^\mathrm{o}$.

## 4.3    PCM phase modulation

The full-transmission metasurface with $w = 420$ nm, $h = 385$ nm, $D = 800$ nm and $n_\mathrm{PCM} = 4$ is now modulated by changing the refractive index of the PCM. The desired response is that of a complete phase coverage with full transmission at a specific work frequency. In Fig.8a, a colour map of the transmittance is given in function of the frequency and the refractive index of the PCM slab. In all the domain, it maintains a close to unity value. Fig.8b shows a phase map for a set of frequencies and $n_\mathrm{PCM}$. For a fixed frequency (i.e. any horizontal line in the surface plots), a full $2\pi$ phase coverage with high transmission is desired. Fig.8c depicts an slice of 8a for the transmittance value and 8b for the phase value, centred at 193 THz. Full-phase coverage is obtained.
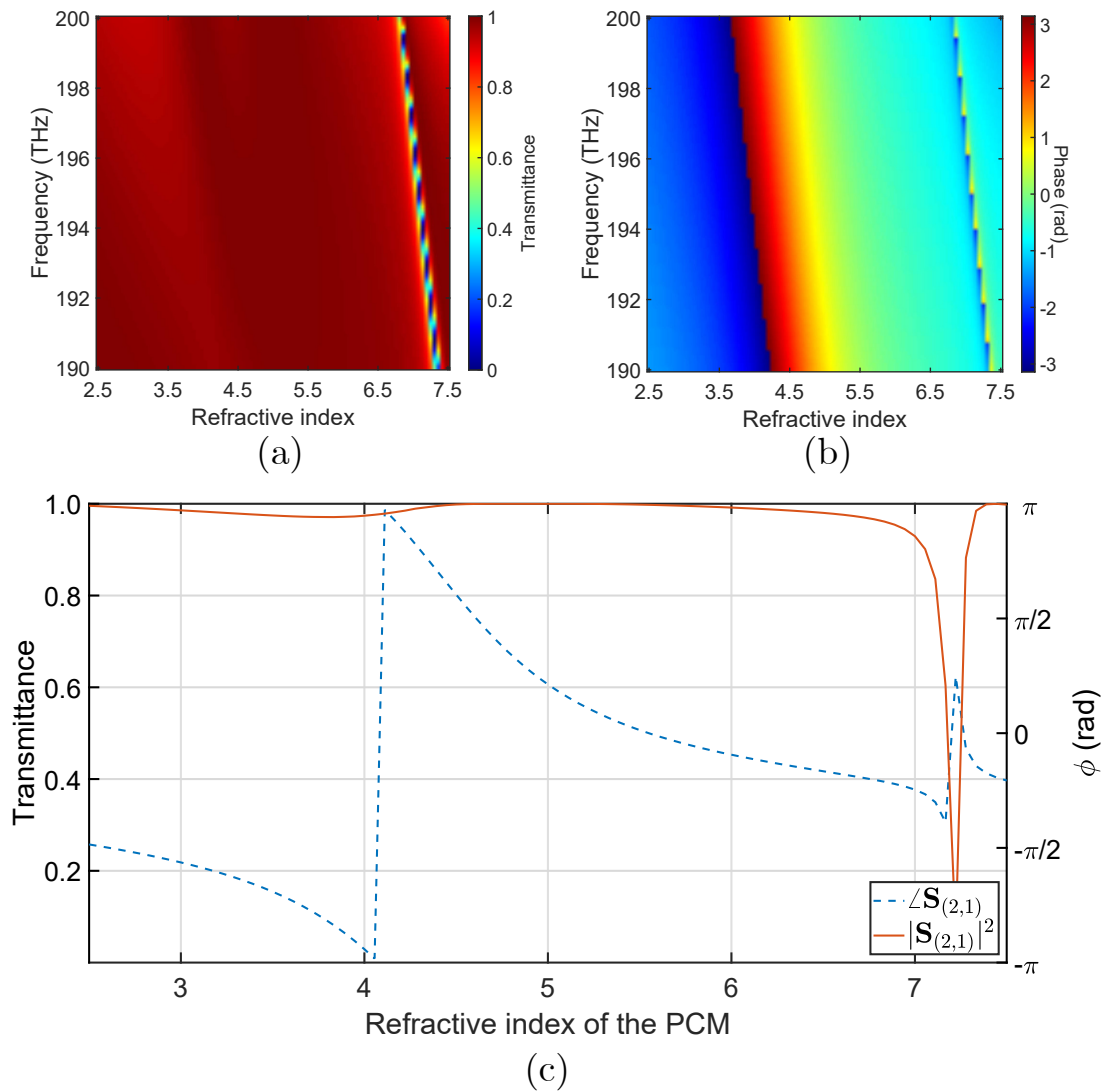
(a)

(b)

(c)

**Figure 8:** (a) Surface plot of the transmittance as a function of the frequency and the PCM's refractive index.  (b) Surface plot of the phase as a function of the frequency and the value of $n_{\text{PCM}}$.(c) Slice of the surface plots above at 193 THz. The transmittance and phase are plotted as a function of $n_{\text{PCM}}$. The geometrical values are the same in every simulation with $D = 800$, $w = 420$nm and $h = 385$nm. Also the values of $n_{\text{d}} = 4$ and $\theta_{\text{i}} = 45^{0}$ were fixed.

# 5 Reconfigurable metasurfaces

## 5.1 Canonical construction of anomalous transmission in Huygens' all-dielectric metasurfaces

Following the generalized law of refraction, a metasurface with a continuous spatial phase gradient can shift incident radiation in any arbitrary direction. The meta-atoms used in the previous section have subwavelength dimensions, but they are not small enough to create an array of them with different phases and claim to have formed a continuous phase shift surface. If the periodicity of the structure is greater than the diffraction limit, higher diffraction orders will appear. Although a greater number of elements in the period can be watched as a higher finesse in the surface phase gradient, the electric dimensions of each resonator remain the same, increasing the period of the metasurface.

The approach to configuring an arrangement of elements capable of steering light is as follows: once fixed the number of elements in the meta-atom cell, with the aid of Fig.8c the refractive index for the needed phase values are found to obtain a $2\pi$ phase coverage in the meta-cell. The expression for the metasurface phase gradient using $N$ number of meta-atoms in the meta-cell with a spacing $D$ is

$$\left| \frac{d\Phi}{dx} \right| = \frac{2\pi}{ND}.$$

(11)

The geometrical parameters of each component are the same in every study of this subsection: $h = 420$ nm, $w = 385$ nm and $D = 800$ nm. It is remarkable that every metasurface studied in this section is physically the same, the only thing that is changing is the state of the PCM in each meta-atom that determines the meta-cell. One important feature, not mentioned yet, is that the structure acts as a non-polarizing device. The geometrical symmetry, the use of isotropic materials and the infinite assumption in the y-axis preserves the polarization state for TM-polarized radiation, defining the TM state as a planewave with only non-zero y-directed component.

The scattering properties of each metasurface configuration will be shown using $|t_m|^2$ and $|r_m|^2$ for the transmittance and reflectance, respectively. The subindex $m$ is the diffraction order of the studied mode, as in Eq.4. Each mode corresponds to a planewave that makes an angle given by the aforementioned equation.

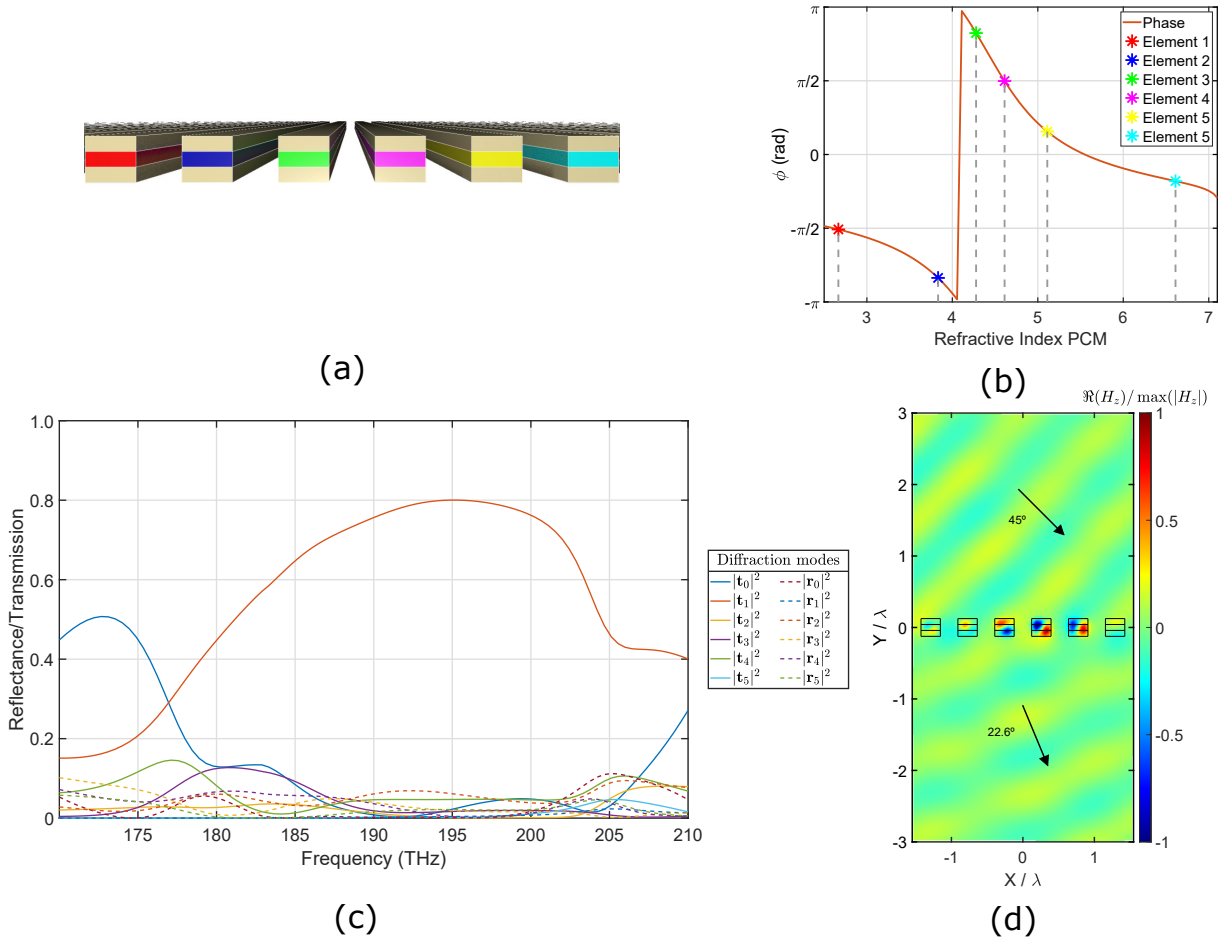### 5.1.1   Anomalous transmission with six elements per period



(a)



(b)



(c)



(d)

**Figure 9:** Anomalous transmission with six elements per period. The refractive indexes
found for the PCM, to cover the entire $2\pi$ phase range, are: $n_1 = 2.7$, $n_2 = 3.8$,
$n_3 = 4.3$, $n_4 = 4.6$, $n_5 = 5.1$ and $n_6 = 6.6$. They are shown in (b) with the model
representation in (a). (c) Shows the scattering properties of the diffraction modes
that the structure supports. The representation of the $H_z$ field at 195 THz is found
in (d). The parameters of the simulation were $w = 420$ nm, $h = 385$ nm, $D = 800$
nm, $n_d = 4$ and $\theta_i = 45^{\underline{o}}$.

This will be the maximum number of meta-atoms that will be modelled in this thesis. The
results obtained are the most efficient with the highest energy coupling to the first order
Floquet (diffraction) mode at 195 THz. In Fig.9c it is shown how the energy couples with
a 80% efficiency to the first Floquet mode. A graphical representation of the periodical
cell is given in 9a and the values for each refractive index of every material are extracted
in Fig.9b. The real part of the Magnetic field, which only has z component, is represented
in Fig.9d. The plane wave can be seen clearly.

### 5.1.2    Anomalous transmission with five elements per period

The five element meta-cell gives a worse performance compared to the previous arrange-
ment (i.e. lower energy coupling to the first diffraction mode). Fewer elements in the
period make a poorer discretization and that is related to the performance of the general-
ized law of diffraction. This trend will continue in the next examples and will be studied
more deeply in the next section.

   In Fig.10a the meta-cell is depicted in a 3D model followed by the refractive index
values for the phase gradient in Fig.10b. Fig.10c shows the response of the metasurface.
The area around 193THz fulfils the theoretical aim of phase gradient and reaches an
energy coupling above 70% for the first Floquet mode. Nevertheless, the plane wave
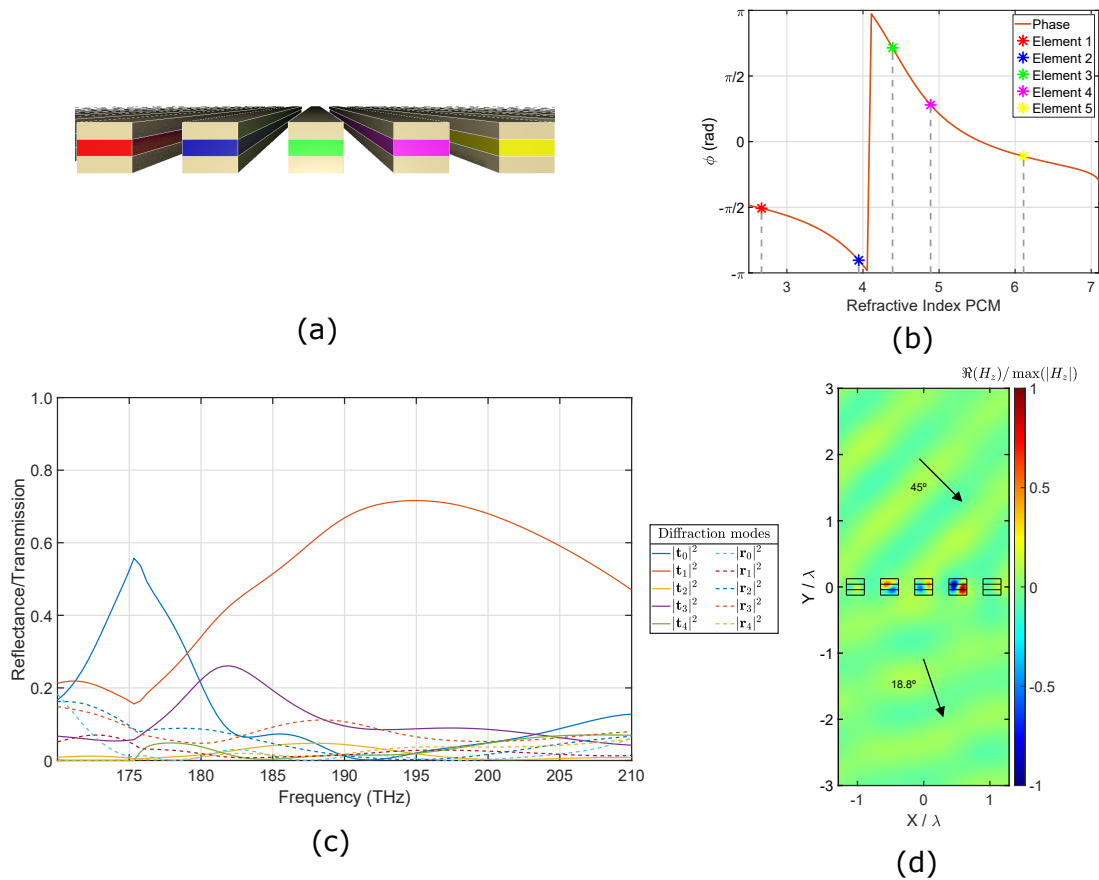propagated suffers interferences with the other propagated modes Fig.10d.



**Figure 10:** Anomalous transmission with five elements per period. (a,b)The obtained
values for the refractive indexes of each element in the meta-cell are $n_1 = 2.7$,
$n_2 = 3.9$, $n_3 = 4.4$, $n_4 = 4.9$ and $n_5 = 6.1$, as shown in .(c) Shows the scattering
properties of the device. (d) Depicts the z-component of the magnetic field at 195
THz. The parameters of the simulation were $w = 420$ nm, $h = 385$ nm, $D = 800$
nm, $n_d = 4$ and $\theta_i = 45^o$.

### 5.1.3    Anomalous transmission with four elements per period
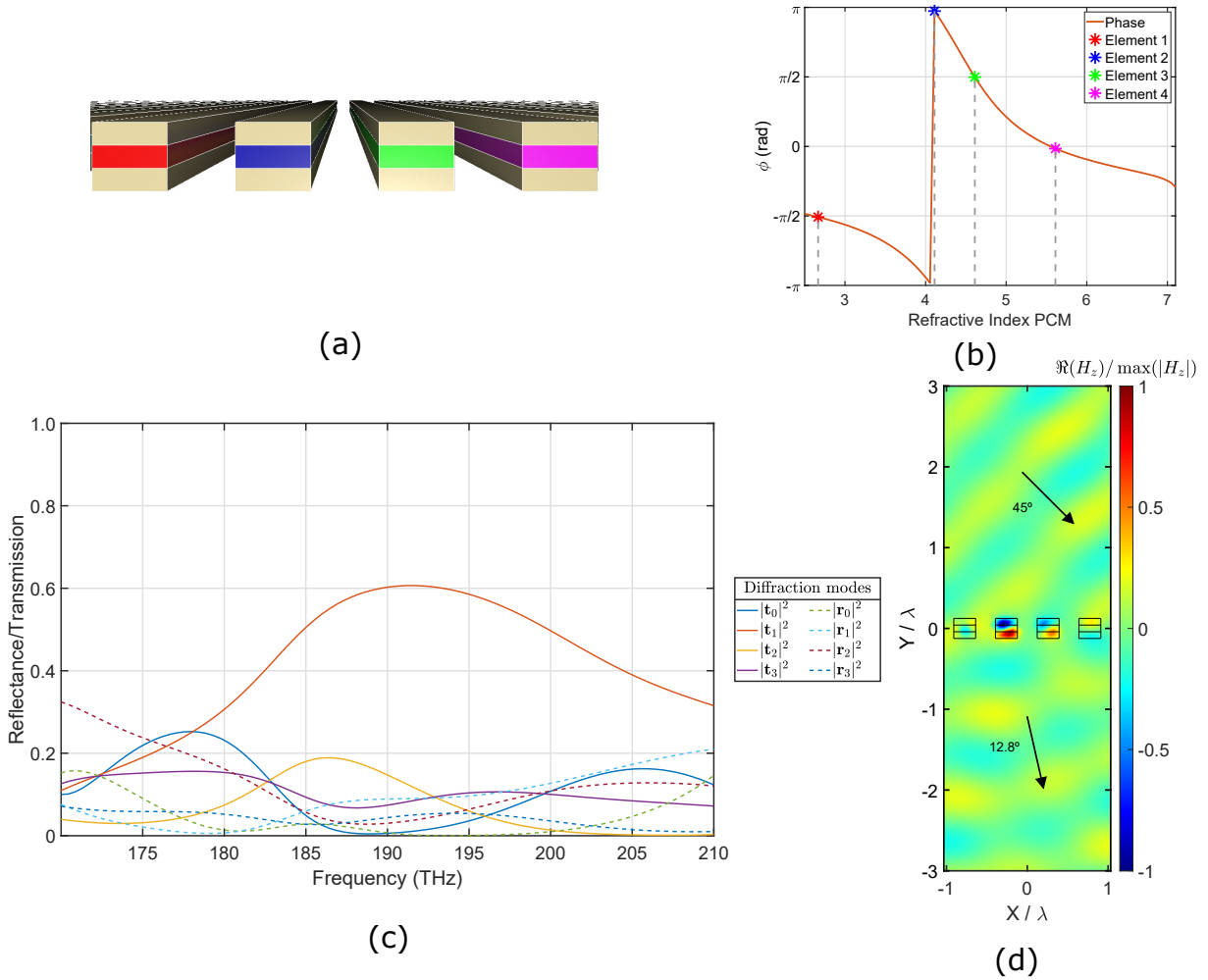


(a)

(b)

(c)

(d)

**Figure 11:** Anomalous transmission with four elements per period. (a-b) The refractive indexes obtained were $n_1 = 2.7$, $n_2 = 4.1$, $n_3 = 4.6$ and $n_4 = 5.6$. (c) Shows the scattering properties of the structure. (d) Depicts the real part of the z component of the magnetic field at 193 THz. The parameters used for the simulation were $w = 420$ nm, $h = 385$ nm, $D = 800$ nm, $n_d = 4$ and $\theta_i = 45^\underline{o}$.

As it was mentioned before the trend continues, poorer discretization makes the continuous assumption of the spatial phase dispersion less applicable. Then the energy coupling is less strong and the generalized law of refraction doesn't hold. Fig.11 depicts, as in the previous cases, a 3D representation of the meta-cell with the study for the indexes values, 11b. The number of propagated modes is lower due to the shorter period of the structure. The energy coupling to the first Floquet mode is still strong at 60% Fig.11c. The field representation is not as clean as it was desired to, Fig.11d. The energy coupling to other propagating modes is significant and there is interference, resulting in a blurred plane wave in the bottom semispace.

### 5.1.4   Anomalous transmission with three elements per period

This last examples shows the limit of the continuous spatial phase assumption in the generalized law of diffraction. Three elements are not enough to behave as a continuous phase change plane. The obtained results can't be explained using the theoretical basis discussed before because none of the made assumptions hold. Fig.12 shows the obtained parameters and disposition of the meta-cell. The scattering parameters are depicted in Fig.12c, a non-clear coupling to any concrete mode is observed.
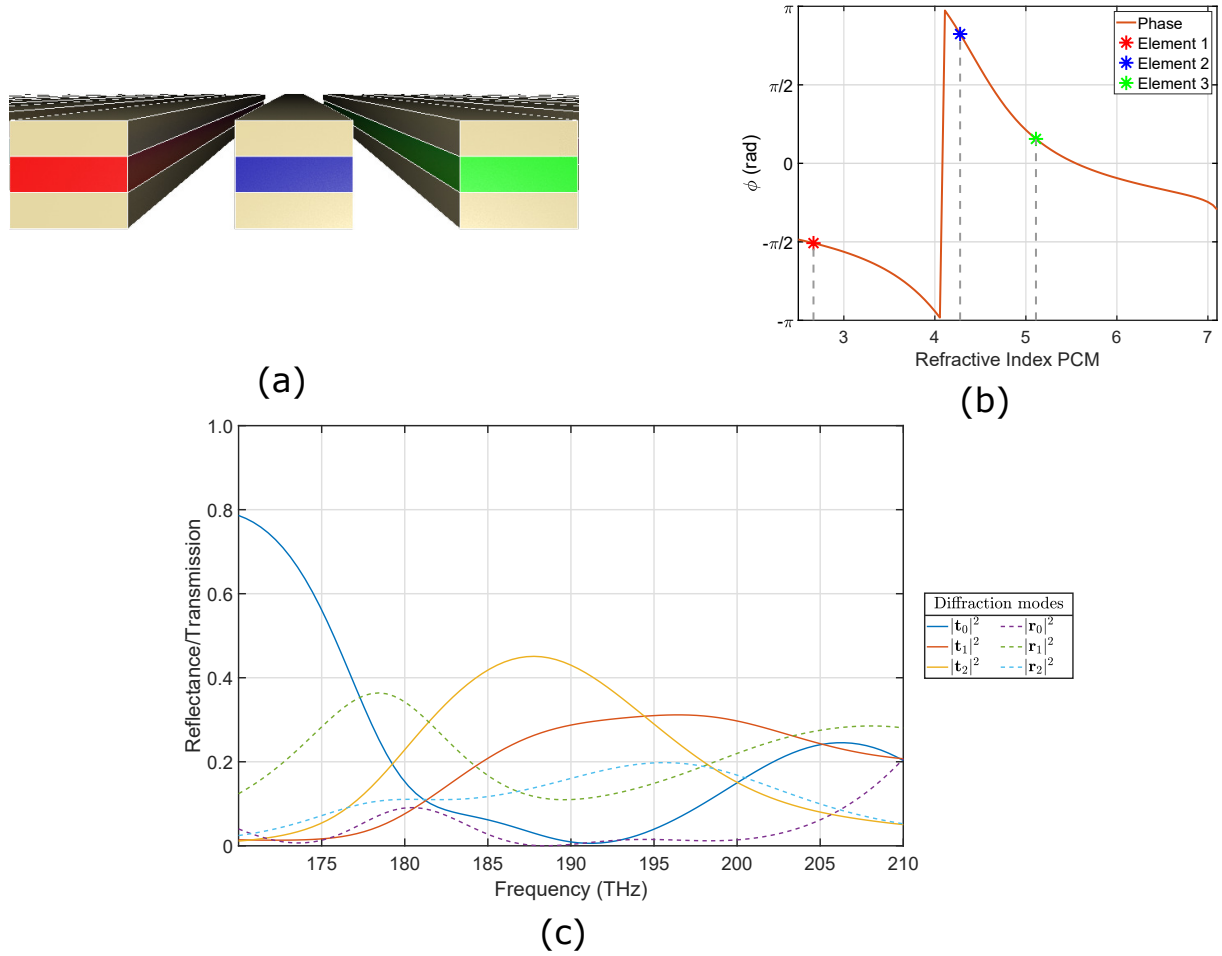


(a)

(b)

(c)

**Figure 12:** Anomalous transmission with three elements per period. (a,b) The obtained values for the 3 elements are $n_1 = 2.7$, $n_2 = 4.3$ and $n_3 = 5.1$. A representation of the sccatering properties of the structure is depicted in (c). The parameters of the simulation were: $w = 420$ nm, $h = 385$ nm, $D = 800$ nm, $n_{\mathrm{d}} = 4$ and $\theta_{\mathrm{i}} = 45^0$

It has been shown how for an increasing number of elements in the meta-cell, the electromagnetic response follows better the generalize law of reflection. From 3 to 6 elements, the efficiencies scaled as 30%, 60%, 70% and 80%. However, only the theoretical approach has been treated so far. It is possible to achieve higher coupling to the first diffraction order using optimization algorithms. Another open question arises, what happends when

the phase gradient changes sign and the equation gives a complex angle. Generally, under normal circumstances, with two homogeneous mediums total internal reflection would be the answer. But in these non perfect gradient, the effects are non trivial and have to be discussed.

Although this section has covered a theoretical approach with perfect conditions simulations, we will not ignore the fact that the dielectric bars have to be sustained by a substrate. This issue will be covered in Section 6, and also the possible experimental realizations.

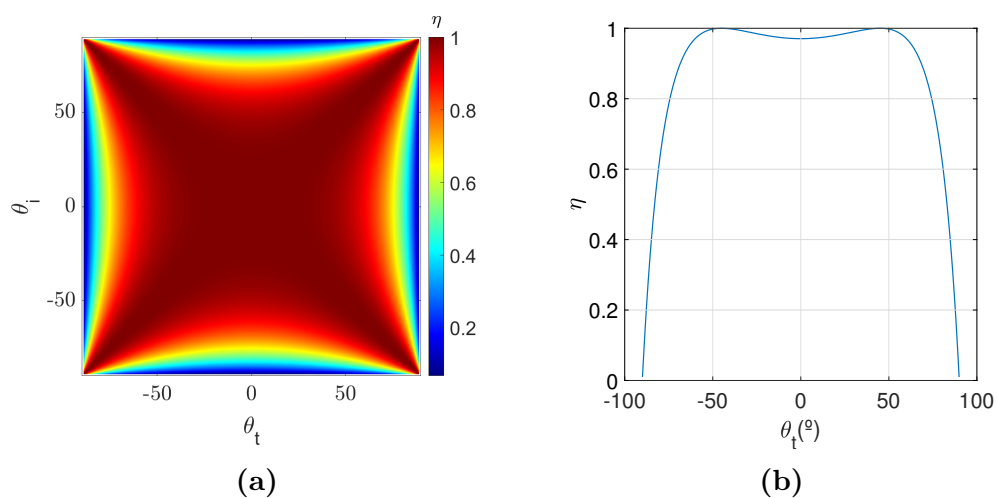## 5.2    Optimization driven metasurface construction



**(a)**                                                          **(b)**

**Figure 13:** (a) Efficiency in terms of incidence angle and transmitted angle. (b) Representation for a fixed incidence angle of $45^{\mathrm{o}}$.

The obtained values for the energy coupling to the first diffraction order, $|t_1|^2$, for the case of 5 and 6 elements are high, but far from the theoretical limit. From [15] we extract the theoretical limit equation for the transmittance energy efficiency

$$\eta = \frac{4\cos\theta_{\mathrm{i}}\cos\theta_{\mathrm{t}}}{(\cos\theta_{\mathrm{i}} + \cos\theta_{\mathrm{t}})^2}, \tag{12}$$

where $\theta_i$ is the angle between between the incident wavevector and the normal plane of the surface and $\theta_t$ is the same angle but for the transmitted wave. This limit is due to the non-adjusted impedances of the incoming and outcoming planewaves. Some of the energy will couple with other modes that are not the first Floquet mode. The studied metasurfaces were design to work with an incidence angle of $45^{\mathrm{o}}$. In Fig.13a we show the surface plot of the efficiency and in Fig.13b the efficiency in terms of the transmitted angle is represented for a fixed $45^{\mathrm{o}}$ incidence angle.
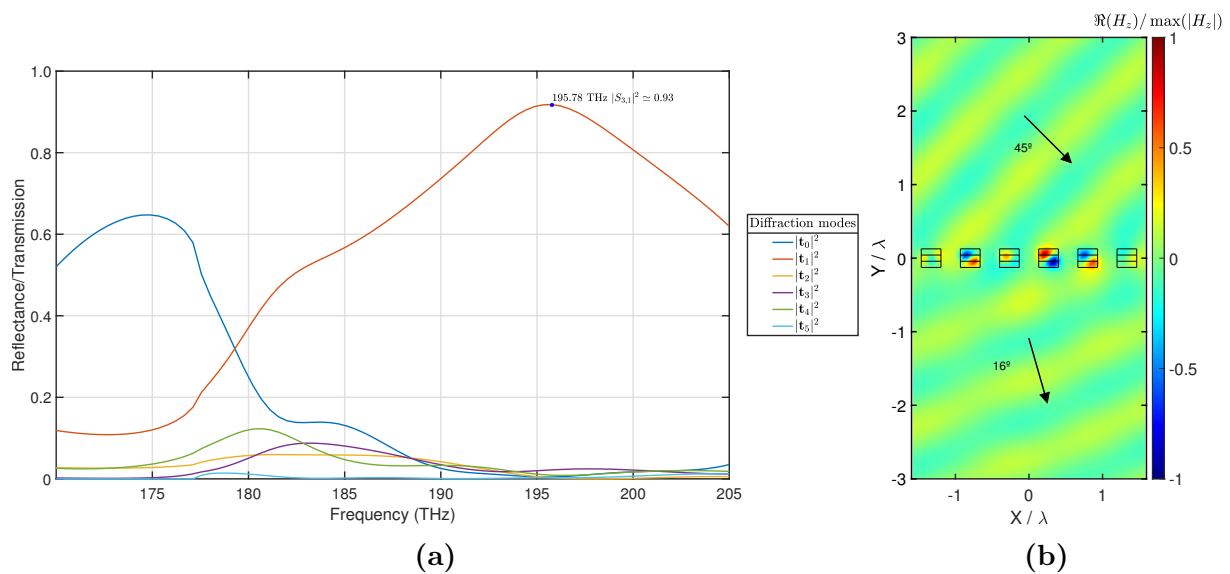
**Figure 14:** Six element optimized meta-cell. (a) Scattering properties of the metasurface in function of the frequency.(b) magnetic field z-component at 193 THz. The values of the simulation were $D = 825$nm, $w = 415$nm, $h = 391$nm, $n_\mathrm{d} = 4$, $\theta_\mathrm{i} = 45$, with the refractive index of each element: $n_1 = 2.9482$, $n_2 = 3.8878$, $n_3 = 4.0317$, $n_4 = 4.511$, $n_5 = 4.9355$ and $n_6 = 6.4807$

Using optimization techniques, the values for $|S_{3,1}|^2$ can be improved greatly. The 5 and 6 element meta cell are optimized applying the Nelder-Mead algorithm. The results depicted in Fig.14 and Fig.15 are closer to the theoretical maximum with a 16% and 24% improvement compare to the results achieved using only the theoretical approach. In both studies the first diffraction order is greatly predominant and thus the field distributions are planewaves with little interference.
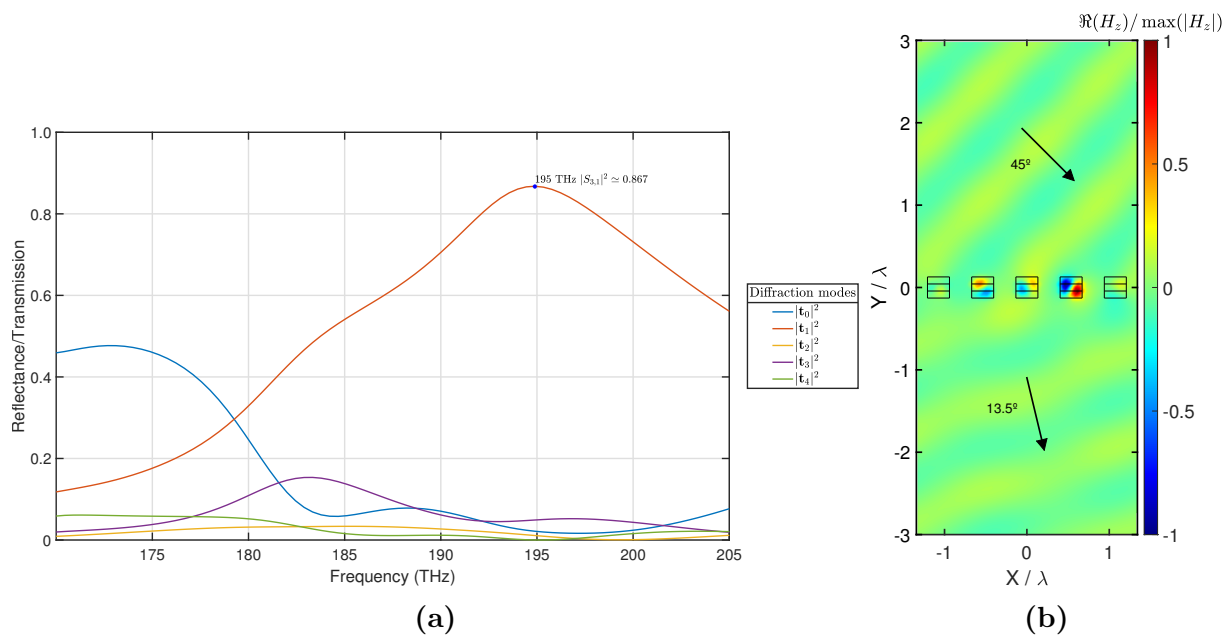
**(a)**                                 **(b)**

**Figure 15:** Five element optimized meta-cell. (a) Scattering properties of the metasurface. (b) Magnetic field z-component. The values of the simulation were $D = 832$nm, $w = 414$nm, $h = 398$nm, $n_d = 4$, $\theta_i = 45$, with the refractive index of each element $n_1 = 3.210$, $n_2 = 3.922$, $n_3 = 4.145$, $n_4 = 4.798$ and $n_5 = 6.036$

Although the performance of the metasurface has been greatly improved with the optimization, the values fall relatively far from the theoretical limits imposed by the impedance mismatch between incident and scattered plane waves. Using Eq.12 we give an overview of the simulated performance relative to the theoretical maximum in Fig.16
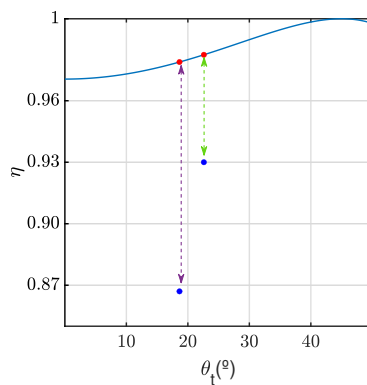


**Figure 16:** The transmission angle gives the theoretical maximum efficiency for the 5 and 6 element meta-cell from left to right, depicted in red in the figure. The blue points are the efficiencies achieved by optimizing the structure from the theoretical starting point.

## 5.3 Discussion and performance limits

The realization of the reconfigurable metasurface for 4, 5 and 6 elements in the meta-cell has been a relative success. In the other hand, the three element meta-cell failed to achieve a high efficiency in energy coupling with the first Floquet mode. Moreover, the trend in efficiency was clear with the number of elements in the cell. The relation was directly proportional. It has already been remarked, but it is interesting to cover one of the main reasons that support the mentioned trend.

Whereas the element size of each resonator remains the same, the number of resonators in the meta-cell affects the fairness of the linear gradient realization, needed to fulfil Eq.5 requirements. To quantify the quality of the discretization, we define the following figure of merit:

$$\alpha = \frac{A_{triangle}}{A_{discretization}}, \tag{13}$$

where $A$ refers to the area below the curve of the theoretical triangles and the poligonal discretization. The linear phase gradient is represented by a triangular function due to the symmetry in the periodicity of the phase, $\phi = \phi + 2\pi n$. The simulated phase is represented by a poligonal step function. Each step is a $D$ size region of a meta-atom where the phase is supposed to be constant.
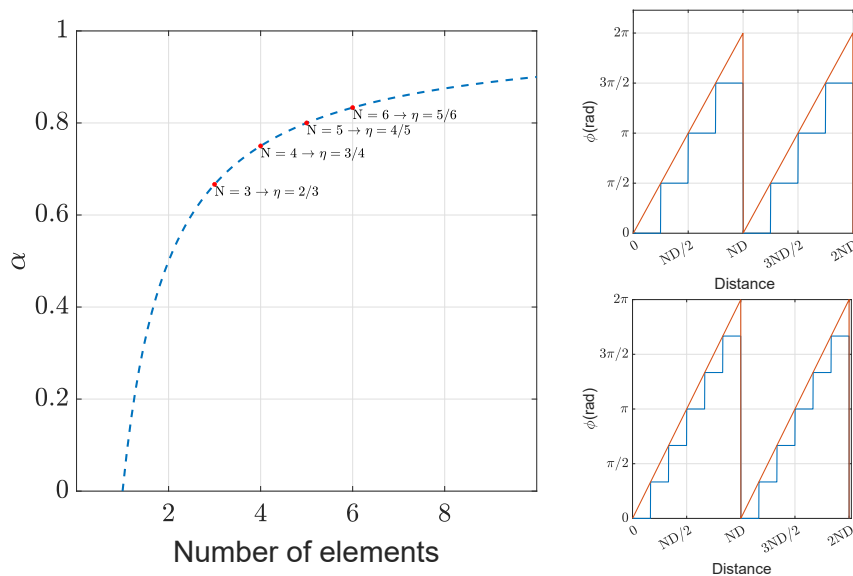


**Figure 17:** The left figure is the representation of Eq.14, the red points are the values for the studied meta-cell in the previous section. The higher the number of elements, the higher the fairness of the linear gradient and thus a higher efficiency in energy coupling to the first Floquet mode. In the right side, two representations of the mentioned areas in Eq.13, specifically in the case of four and six elements in the cell.

The Eq.13 can be easily work out theoretically using simple geometry. The result

proves what the graphical intuition provides:

$$\alpha = \frac{N-1}{N},\tag{14}$$

the equation only depends on the number of elements in the meta-cell, $N$, and not in the dimensions of each meta-atom $D$, or even in the periodicity dimensions of the cell, $ND$. In Fig.17 the curve in Eq.14a is plotted with the studied cases marked. Two examples are graph in Eq.14(b)(c) where the horizontal axis is the x-axis distance of the metasurface and $\phi$ represents the phase introduced by the resonators in blue, and the perfect phase needed depicted in orange.

This study supports quantitatively the relation between the number of elements in the period and a better approach to a linear phase function in the x-dimension, then a better coupling in energy to the first diffraction mode. Nevertheless, the discretization of the continuous phase gradient is not the only aspect that affects the efficiency of the whole structure. Another well documented issue is that this type of metasurfaces suffer from non-local effects. During the previous sections, we have treated, in theoretical design, each individual resonator as an isolated resonator whose response only depends on itself and not in the way that is arrange in the periodical structure. Indeed, we have neglected the effect of the evanescent fields created by neighbour resonators to calculate the phase required to create a linear phase shift.

Taking into account the effects of adjacent resonators is not an easy task. Moreover, guided modes could even propagate at certain frequencies and dimensions. These effects are usually viewed as non-local. Non-locality refers to the effects that arise in metasurfaces which cannot be explained in terms of the individual meta-atoms. More formally, we refer to local metasurfaces when the response of the structure can be explained by pointwise spatial information [16]. In the other hand, we call non-local metasurfaces to those whose response can not be fully explained by the spatial information of the structure.

In the case of study of this master's thesis, the spatial property that has been spatially modulated is the phase. For the cases above the behaviour of the working metasurfaces can be explained only by this spatial property. The phase changes in an approximately linear way and thus the response is that the energy is redirected to the first diffracted mode, as the Generalized law of refraction states. The non-perfect coupling can be explained with the above study of the discretization fairness. In which it has been proven that a better fit to the linear behaviour relates with a better performance in energy coupling. Evidently, there is coupling between the meta-atoms and that also affects the performance, but it is not the major source of error.

An uncomplicated way of exploring the metasurface response behaving as a non-local device, is changing the sign of the spatial phase gradient. This can be done by inverting the order of each resonator in the meta cell. In that case the generalized law of refraction would yield a complex angle. The general interpretation of complex angles is that total internal reflection is happening and the complex part relates inversely to the evanescent wave penetration distance. The energy should be redirected into the reflected ray entirely, if we were dealing with a two medium standard system. We will show examples where other Floquet modes, different from the first, are excited.
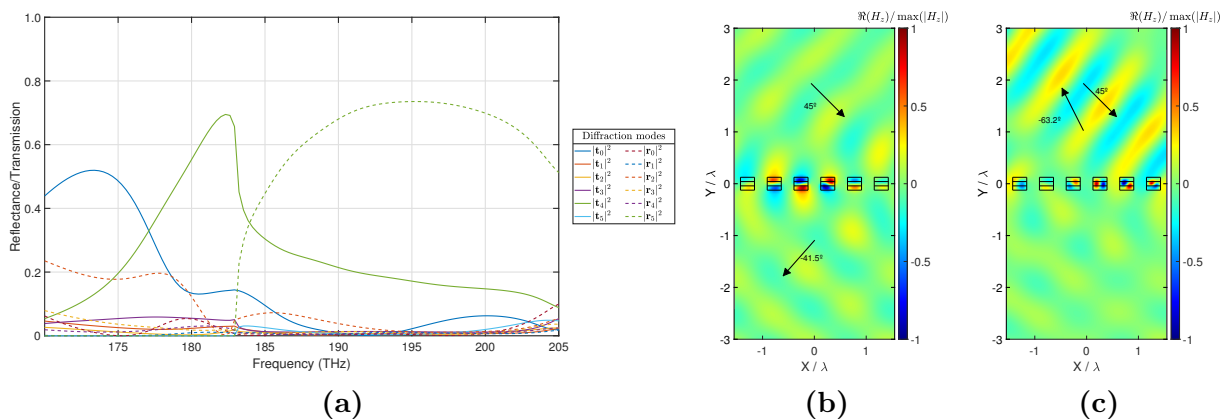
**Figure 18:** Six element meta-cell with non local behaviour. (a) Scattering properties of the structure. (b) $H_z$ field at 180.67 Thz of the current configuration. (c) Magnetic field depiction at 195.33 THz. The parameters of the simulation were $w = 420$nm, $h = 385$nm, $D = 800$nm, $n_d = 4$ and $\theta_i = 45^o$, with $n_6 = 2.7$, $n_5 = 3.8$, $n_4 = 4.3$, $n_3 = 4.6$, $n_2 = 5.1$ and $n_1 = 6.6$.

The results obtained cannot be explained only by the pointwise spatial information. Therefore the configurations are considered to have a non-local response. Two interesting results are shown for the six-element and four-element meta-cell. In Fig.18a the modal distribution of energy is depicted for the six-element meta-cell with a negative spatial phase gradient. Two interesting peaks are found at around 180 THz and 195 THz, the first one corresponds to m=4 at transmission, and the second corresponds to m=5 at reflection, both of them with a 70% energy coupling. The field distributions for the magnetic z-component are shown in 18(b,c)

Another promising non-local metasurface is the four-element meta-cell with constant negative gradient that at 187 THz works as a retroreflector with almost 90% efficiency in Fig.19a. The energy couples to the third diffraction order in reflection and the field distribution in the superior half-plane is a perfectly matched ingoing $45^o$ plane wave with an outgoing $45^o$ plane wave, see Fig.19b.
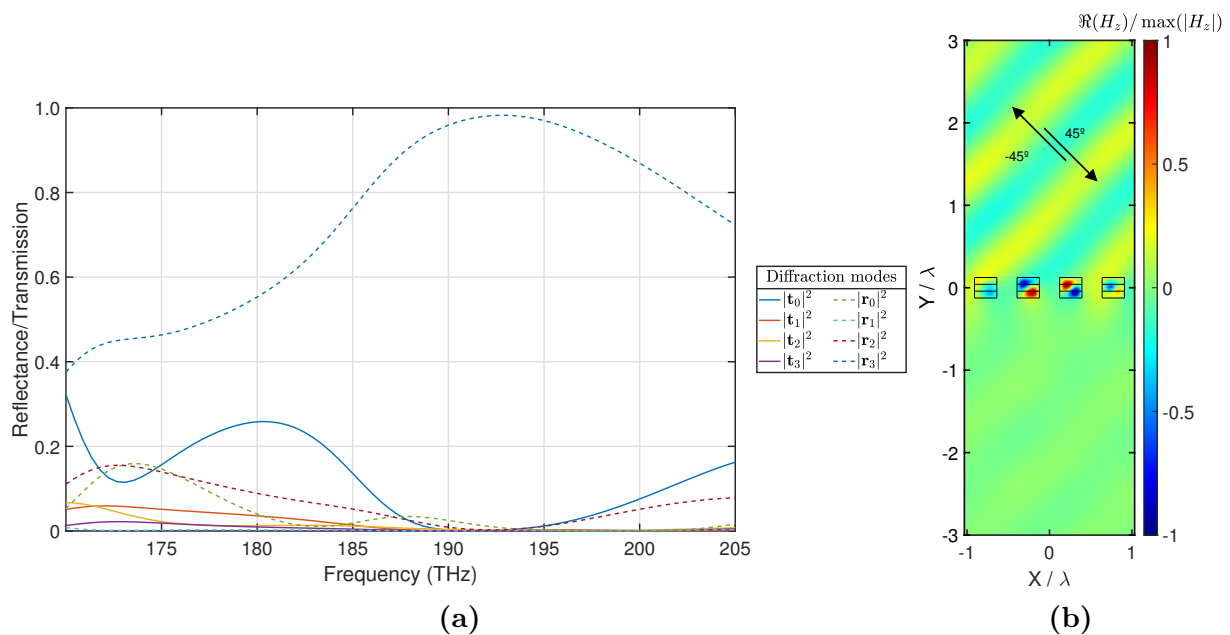
**Figure 19:** Four element meta-cell with non local behaviour. (a) Scattering properties of the structure. (b) $H_z$ field at 197.56 THz of the current configuration. The parameters of the simulation were $w = 420$ nm, $h = 385$ nm, $D = 800$ nm, $n_{\mathrm{d}} = 4$ and $\theta_{\mathrm{i}} = 45^{\mathrm{o}}$, with $n_4 = 2.7$, $n_3 = 4.1$ , $n_2 = 4.6$ and $n_1 = 5.6$.

# 6    Simulations of a realistic structure

We have demonstrated the possibility of creating a reconfigurable metasurface with the use of a PCM (phase change material). The theoretical working principle has been covered, and it has worked properly in the simulations made. In this section, we are going to bring the simulations closer to what could be made with the current technology in the NTC facilities.

The most important issues to cover are the choice made for the substrate of the dielectric bars and the PCM that will be used. The dielectric bars have been treated as floating in the air. The simulation should be made using a substrate as the holder of the device to achieve a more realistic situation. Because of its high transparency in the NIR, the CaF$_2$, calcium fluoride, is often used as the substrate [17]. The refractive index of this material at $\lambda = 1550$ nm and $20^{\mathrm{o}}$C, is $n_{(CaF_2)} = 1.4261$ with negligible losses [18]. As expected, the use of a material with a different refractive index in the lower half-plane breaks the symmetry of the whole geometry.

Moreover, changing air to calcium fluoride leads to a worse index contrast between the dielectric pillars and their environment. Therefore the confinement of the field and thus the resonances Q factors are significantly affected. In order to solve the problems presented, a correction in structure's geometry must be made.

Another missing piece in the scheme is the choice of the PCM material. From all the materials with PCM characteristics, the family of materials labelled GST (Ge-Sb-Te) is

one more promising for our structure. The best quality that the GST family shares is their non-volatile character [19]. This means that once made the modification in their internal structure, it remains permanent until it is altered again. GST's internal structure changes with the interaction with light, voltages or temperature [6]. Their internal structure can change from amorphous (a-GST) to crystalline (c-GST). Between those two states, there can be intermediate stages with different levels of crystallization. The lower refractive index is found in the amorphous stage, and it increases when the crystallization state approaches its maximum.

It is also time to address one important issue, which is transversal to all matter when illuminated with light, losses. Usually, the materials chosen to form an structure are those that have negligible losses to avoid dissipation of energy and quality factor drops. In the case of GST materials, losses are unavoidable. But they can be minimized. Minimizing losses requires working at higher wavelengths and with certain materials from the GST family.

## 6.1    Effect of the supporting substrate and the PMC thickness

The simulation of the substrate creates asymmetry in the structure, and it also decreases the index contrast between the resonators and their surroundings. Therefore, the geometry of the dielectric bars has to be changed to take into account this new configuration. The line of thought, and the methodology, is the same as in Section 4. As we have discussed how to achieve the full transmission condition previously, this section presents only a brief summary with the results achieved of this new configuration. Fig.20a shows the squared absolute value of the S-parameters in the structure. Due to the inclusion of the substrate, the diffraction limit is set at a lower frequency. In the figure is easy to see how at 195THz the diffraction limit is reached and a higher than zero order Floquet mode appears. Following the same approach as in Section 3, the superposition of both electric dipole resonances is needed to obtain high transmission. When the structure is illuminated by a TM-polarized plane wave with an incidence angle of $45^{\text{o}}$, the obtained transmission value is above 90% but not the full transmission of the case without substrate. Fig.20b shows the resonance at 180 THz where both dipoles have the same amplitude and phase. The last graph, Fig.20c, shows the transmission and phase of the $S_{(2,1)} = t_1$ parameter. Not a full phase coverage is achieved, but it is sufficient to implement the discrete meta-cells.

Due to the higher refractive index of the calcium fluoride, the diffraction limit is surpassed at lower frequencies. The periodicity of the structure has to be changed to stay only with the first order of diffraction. A lower $D$ implies higher cut frequencies for higher order Floquet modes. In addition, the resonances are less confined and thus, they present lower Q factors and broader resonances. The $x$-dimension, $w$, and $z$-dimension, $h$, have to be increased in order to avoid the field in the substrate moving the resonances at lower frequencies.
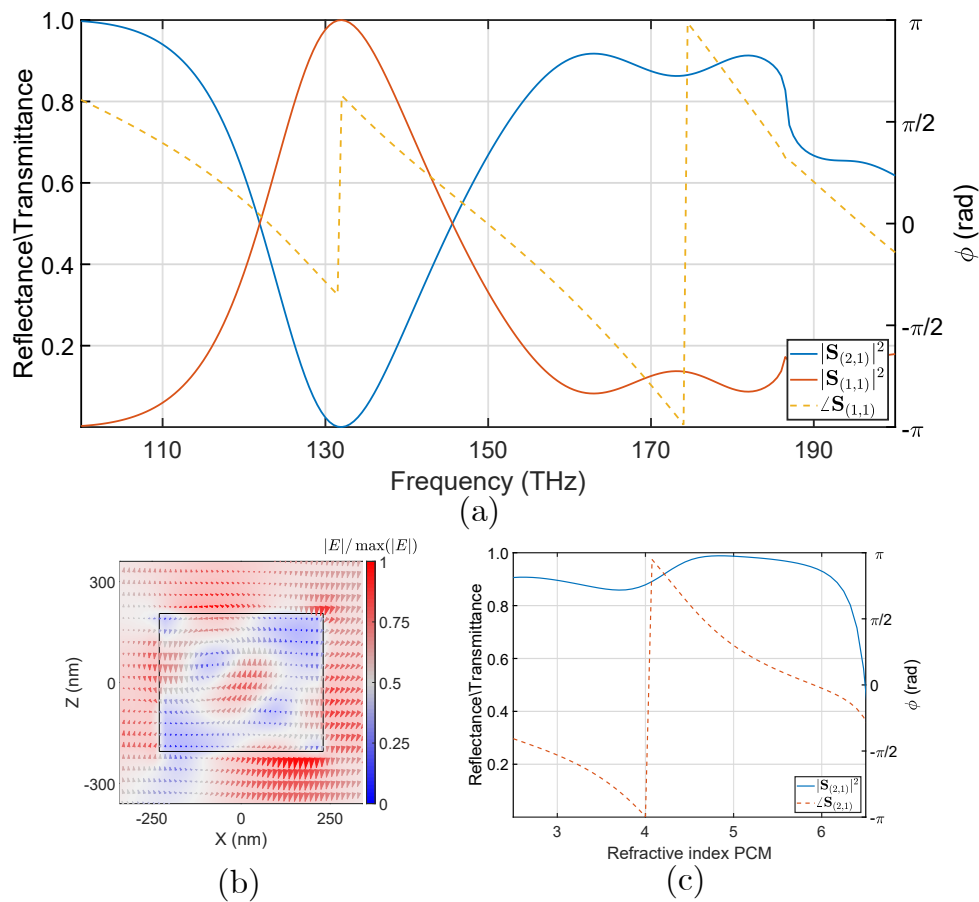
**Figure 20:** One element metasurface with calcium flouride substrate. (a) Scattering properties with geometrical values: $w = 460$ nm, $h = 410$ nm, and $D = 720$ nm, frequency study when $n_\mathrm{d} = 4$. (b) Representation of the electric field distribution at 180 THz. (c) The refractive index of the PCM is modulated achieving a full $2\pi$ phase coverage at 180 THz.

Another substantial change has to be made in the geometry for a practical purpose: the height of the PMC layer was increased to $h_\mathrm{PCM} = 2h/5$ from the $h_\mathrm{PCM} = h/3$ in the metasurface without substrate. This is a direct consequence of the decrease in index contrast. A bigger slab of PCM greatly impacts the modulation of the dipoles, especially in the strength of the electric dipole in the $x$ direction. This will also mean that the frequency of resonance of the $x$ directed dipole will change more with the modulation of the refractive index. Then the phase coverage can be achieved with a more minor variation of the refraction index of the PMC material as is presented in Fig.20c.
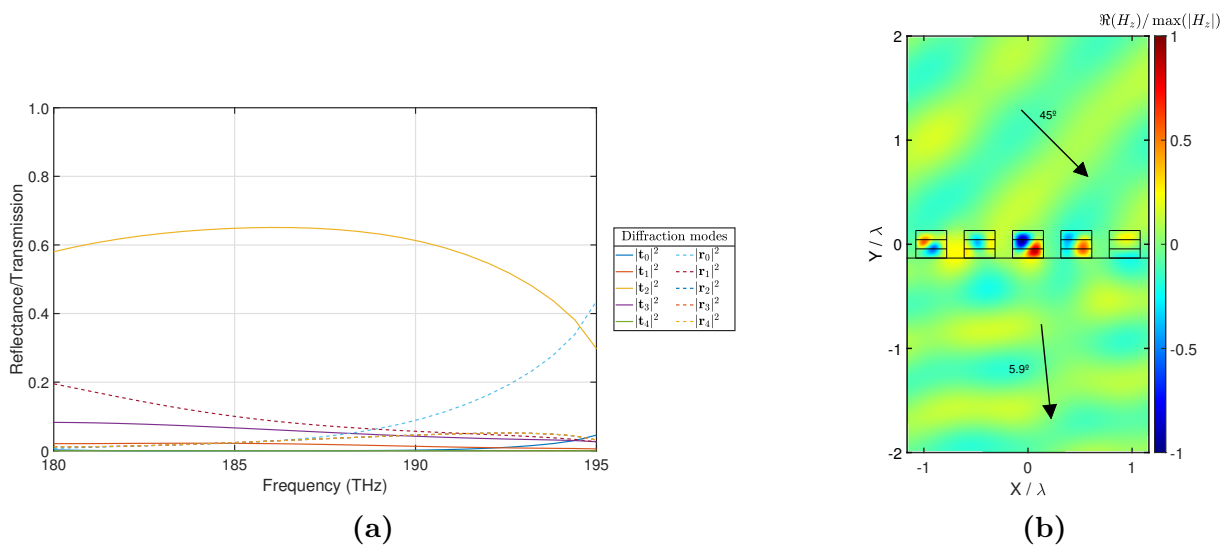
**Figure 21:** Five element metasurface with calcium fluoride substrate. (a) Scattering
properties at different frequencies of a metasurface with five elements per period
when $D = 720$, $w = 460$nm, $h = 410$nm, $h_{\mathrm{PCM}} = 2/5h$, $\theta_{\mathrm{i}} = 45^{\mathrm{o}}$. With indexes:
$n_1 = 2.74$, $n_2 = 3.65$ , $n_3 = 4.14$, $n_4 = 4.76$ and $n_5 = 5.74$. (b) Magnetic field plot.
Performance of the metasurface at 186 THz.

A demonstration of the functionality of a gradient metasurface with five elements and
this new configuration is shown in Fig.21a. The energy that couples to the first Floquet
mode is above 60% and there is a steering of the incident wave of more than $39^{\mathrm{o}}$. Notice
that this deviation is greater than the achieved in the metasurface without substrate. This
is due to the higher refractive index in the second media. The magnetic field distribution
showing this performance is represented in Fig.21b at 186 THz.

## 6.2    Effect of dielectric losses in the structure

Gathering the knowledge acquired in the development of this master's thesis, a closer-
to-reality simulation of a reconfigurable metasurface is presented in this section. The
addition of the substrate, the losses and the use of a real material are going to be modelled.
Nevertheless, the construction imperfections are neglected. We would also consider that
the accessible states between a-GST and c-GST are sufficient to cover our specifications
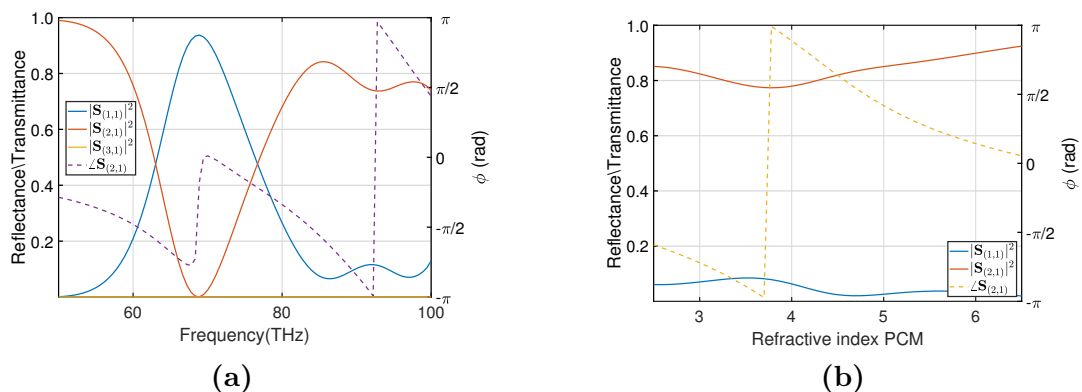in the refractive index.

**Figure 22:** Response of the homogeneous metasurface with dielectric losses.(a) Scattering properties of the structure in terms of the frequency. Geometrical parameters: $h = 800$nm, $w = 900$nm, and $D = 1400$nm. The slab of GST is 1/7 of the height, $h_{\text{PCM}} = 1/7h$. And the refractive index of germanium at 80 THz is taken as $n_{\text{d}} = 4.0447$. (b) Scattering properties for different values of the refractive index of the GST slab for 91.8 THz with an extinction coefficient of $k = 0.05$.

As demonstrated experimentally [6], there are many accessible non-volatile states of relative crystallization in $Ge_3Sb_2Te_6$, a material of the GST family. The counterpart of using this material is that the extinction coefficient is only assumable in the mid-IR. We will adapt the design to work in the range of $(2.5\text{-}5)\mu$m. This will mean going from around 193 THz to (120-60) THz in the frequency domain. The extinction coefficient of $Ge_3Sb_2Te_6$ , $k$, varies from 0.1 to 0.7 for $\lambda > 3.5\mu m$, depending on the crystallization state that the material presents [6]. In addition, in order to facilitate the change between different crystallization states, the slab of GST is only 1/7 of the height.

Fig.22a shows the response achieved by the $45^{\text{o}}$ electric dipole using a $n_{\text{PCM}} = 4$ with an extinction coefficient of $k_{\text{PCM}} = 0.1$. The obtained values are below unity for transmittance due to the absorption in the structure. Losses and asymmetry are the sources of these lower values. The phase coverage is studied in Fig.22, showing that it is below $2\pi$ but greater than $3/2\pi$. The reduction in the phase coverage is mainly caused by the decrease in the height of the GST layer. This phase coverage can be enough for some meta-cell arrangements.

# 7   Conclusion

During the realization of this thesis, it has been shown a mechanism to reconfigure an all-dielectric Huygens metasurface with only electrical response using phase change materials. The geometry studied in this thesis allows achieving full transmission with two electric dipole Mie-type resonances that formed a $90^{\text{o}}$ angle, fulfilling the first Kerker condition. A full $2\pi$ phase coverage was achieved by modulating the refractive index of the PCM slab in the infinite dielectric bar architecture. Using the information extracted from the analysis of the homogeneous metasurface, n-elements meta-cells were designed for coupling the energy into the first diffraction mode, as the generalized law of diffraction states. The results were satisfactory; the reconfiguration process was achieved with high energy efficiency.

The efficiency of each metasurface arrangement grew with the number of elements in the meta-cell. The trend was supported theoretically by studying the fitness of the meta-cell to a linear phase function in the x-spatial direction. Furthermore, starting from the theoretical arrangement of refractive indexes, an optimization algorithm was used in order to achieve better performance. It is well known that computational optimization does not allow a better understanding of the physical principles behind the structure's electromagnetic response. Still, it serves to close the gap between the obtained performance and the theoretical maximum.

Exploiting the non-local properties that subwavelength structures can support [16], some non-local metasurface configurations were proposed. Another step that the study took was the approach to a realistic configuration of the metasurface. A realistic physical model, including the effect of the supporting substrate and dielectric losses, was made with relative success. The introduction of losses made unity transmission impossible, and the phase coverage was reduced. Moreover, an actual well-studied non-volatile PCM was proposed, $Ge_3Sb_2Te_6$, which properties had been studied in the mid-IR range [6, 19]. The metasurface was adapted to work at lower frequencies to avoid the high losses of GST-family materials in the NIR. The mechanism of reconfiguration is simple, through laser pulses the crystallization state can be changed between low-refractive-index a-GST (amorphous) to high-refractive-index c-GST (crystal), as demonstrated experimentally in [20].

# 8   Acknowledgements

# References

[1] N. Yu, P. Genevet, M. A. Kats, F. Aieta, J.-P. Tetienne, F. Capasso, and Z. Gaburro, "Light propagation with phase discontinuities: Generalized laws of reflection and refraction," Science, vol. 334, no. 6054, pp. 333–337, 2011. [Online]. Available: https://www.science.org/doi/abs/10.1126/science.1210713

[2] A. A, H. Y, and B. M. F. A., "Dielectric metasurfaces for complete control of phase and polarization with subwavelength spatial resolution and high transmission," Nature Nanotechnology, vol. 10, pp. 937–943, 2015. [Online]. Available: https://doi.org/10.1038/nnano.2015.186

[3] O. Quevedo-Teruel, H. Chen, A. Díaz-Rubio, G. Gok, A. Grbic, G. Minatti, E. Martini, S. Maci, G. V. Eleftheriades, M. Chen, N. I. Zheludev, N. Papasimakis, S. Choudhury, Z. A. Kudyshev, S. Saha, H. Reddy, A. Boltasseva, V. M. Shalaev, A. V. Kildishev, D. Sievenpiper, C. Caloz, A. Alù, Q. He, L. Zhou, G. Valerio, E. Rajo-Iglesias, Z. Sipus, F. Mesa, R. Rodríguez-Berral, F. Medina, V. Asadchy, S. Tretyakov, and C. Craeye, "Roadmap on metasurfaces," Journal of Optics, vol. 21, 2019. [Online]. Available: https://iopscience.iop.org/article/10.1088/2040-8986/ab161d

[4] Z. Guanxing, Z. Liu, W. Deng, and W. Zhu, "Reconfigurable metasurfaces with mechanical actuations: towards flexible and tunable photonic devices," Journal of Optics, vol. 23, 2021.

[5] M. R. Eskandari, M. A. Shameli, and R. Safian, "Analysis of an electrically reconfigurable metasurface for manipulating polarization of near-infrared light," J. Opt. Soc. Am. B, vol. 39, no. 1, pp. 145–154, Jan 2022. [Online]. Available: http://opg.optica.org/josab/abstract.cfm?URI=josab-39-1-145

[6] A. Leitis, A. Heßler, S. Wahl, M. Wuttig, T. Taubner, A. Tittl, and H. Altug, "All-dielectric programmable huygens' metasurfaces," Advanced Functional Materials, vol. 30, no. 19, p. 1910259, 2020. [Online]. Available: https://onlinelibrary.wiley.com/doi/abs/10.1002/adfm.201910259

[7] C. R. de Galarreta, A. M. Alexeev, Y.-Y. Au, M. Lopez-Garcia, M. Klemm, M. Cryan, J. Bertolotti, and C. D. Wright, "Nonvolatile reconfigurable phase-change metadevices for beam steering in the near infrared," Advanced Functional Materials, vol. 28, no. 10, 2018. [Online]. Available: https://onlinelibrary.wiley.com/doi/abs/10.1002/adfm.201704993

[8] X. Wang, "Metasurface-impedance engineering for advanced wave transformations," Ph.D. dissertation, Aalto University, Espoo, Finland, may 2020.

[9] C. Simovski and S. Tretyakov, An Introduction to Metamaterials and Nanophotonics, 1st ed. Cambridge University Press, 2020.

[10] V. S. Asadchy, A. Díaz-Rubio, and S. A. Tretyakov, "Bianisotropic metasurfaces: physics and applications," Nanophotonics, vol. 7, no. 6, pp. 1069–1094, 2018. [Online]. Available: https://doi.org/10.1515/nanoph-2017-0132

[11] S. Larouche and D. R. Smith, "Reconciliation of generalized refraction with diffraction theory," Opt. Lett., vol. 37, no. 12, pp. 2391–2393, Jun 2012. [Online]. Available: http://opg.optica.org/ol/abstract.cfm?URI=ol-37-12-2391

[12] F. Papoff and B. Hourahine, "Geometrical mie theory for resonances in nanoparticles of any shape," Opt. Express, vol. 19, no. 22, pp. 21 432–21 444, Oct 2011. [Online]. Available: http://opg.optica.org/oe/abstract.cfm?URI=oe-19-22-21432

[13] A. Epstein and G. V. Eleftheriades, "Huygens metasurfaces via the equivalence principle: design and applications," J. Opt. Soc. Am. B, vol. 33, no. 2, pp. A31–A50, Feb 2016. [Online]. Available: http://opg.optica.org/josab/abstract.cfm?URI=josab-33-2-A31

[14] D.-H. Kwon, G. Ptitcyn, A. Díaz-Rubio, and S. A. Tretyakov, "Transmission magnitude and phase control for polarization-preserving reflectionless metasurfaces," Phys. Rev. Applied, vol. 9, p. 034005, Mar 2018. [Online]. Available: https://link.aps.org/doi/10.1103/PhysRevApplied.9.034005

[15] A. Díaz-Rubio, V. S. Asadchy, A. Elsakka, and S. A. Tretyakov, "From the generalized reflection law to the realization of perfect anomalous reflectors," Science Advances, vol. 3, no. 8, 2017. [Online]. Available: https://www.science.org/doi/abs/10.1126/sciadv.1602714

[16] A. Overvig and A. Alù, "Diffractive nonlocal metasurfaces," Laser & Photonics Reviews, vol. 16, no. 8, p. 2100633, 2022. [Online]. Available: https://onlinelibrary.wiley.com/doi/abs/10.1002/lpor.202100633

[17] F. Shen, Q. Kang, J. Wang, K. Guo, Q. Zhou, and Z. Guo, "Dielectric metasurface-based high-efficiency mid-infrared optical filter," Nanomaterials, vol. 8, no. 11, 2018. [Online]. Available: https://www.mdpi.com/2079-4991/8/11/938

[18] M. Daimon and A. Masumura, "High-accuracy measurements of the refractive index and its temperature coefficient of calcium fluoride in a wide wavelength range from 138 to 2326 nm." Applied optics, vol. 41 25, pp. 5275–81, 2002.

[19] Z. Xu, C. Chen, Z. Wang, K. Wu, H. Chong, and H. Ye, "Optical constants acquisition and phase change properties of ge2sb2te5 thin films based on spectroscopy," RSC Adv., vol. 8, pp. 21 040–21 046, 2018. [Online]. Available: http://dx.doi.org/10.1039/C8RA01382A

[20] Y. Wang, P. Landreman, D. Schoen, K. Okabe, A. Marshall, U. Celano, H.-S. P. Wong, J. Park, and M. L. Brongersma, "Electrical tuning of phase-change antennas and metasurfaces," Nature Nanotechnology, vol. 16, pp. 667–672, 2021. [Online]. Available: https://doi.org/10.1038/s41565-021-00882-8